Western Graduate&PostdoctoralStudies

Western University
Scholarship@Western

Electronic Thesis and Dissertation Repository

1-20-2017 12:00 AM

Histological Quantification in Temporal Lobe Epilepsy

Charlotte Anne Blinston
The University of Western Ontario"

Supervisor
Dr Terry Peters
The University of Western Ontario Joint Supervisor
Dr Ali Khan
The University of Western Ontario

Graduate Program in Biomedical Engineering
A thesis submitted in partial fulfillment of the requirements for the degree in Master of Engineering Science
© Charlotte Anne Blinston 2017

Follow this and additional works at: https://ir.lib.uwo.ca/etd

 Part of the Other Biomedical Engineering and Bioengineering Commons

Recommended Citation

Blinston, Charlotte Anne, "Histological Quantification in Temporal Lobe Epilepsy" (2017). *Electronic Thesis and Dissertation Repository*. 4394.
https://ir.lib.uwo.ca/etd/4394

This Dissertation/Thesis is brought to you for free and open access by Scholarship@Western. It has been accepted for inclusion in Electronic Thesis and Dissertation Repository by an authorized administrator of Scholarship@Western. For more information, please contact wlswadmin@uwo.ca.

www.manaraa.com

Abstract

Approximately 30 percent of epilepsy patients suffer from refractory temporal lobe epilepsy which is commonly treated with resection of the epileptogenic tissue. However, surgical treatment presents many challenges in locating the epileptogenic focus and thus not all patients become seizure-free following surgery. Advances in techniques can lead to improved localization of the epileptogenic zone and may be validated by correlating MRI with neuropathology of the excised cortical tissue. Focal cortical dysplasias are a neuropathological group of cortical malformations that are often found in cases of refractory epilepsy, however, they are subtle and difficult to quantify. The purpose of this research is to employ histology image analysis techniques to better characterize these abnormalities at the neuronal and laminar level, allowing for correlative MRI-histology studies and improved lesion detection in medically intractable TLE.

Keywords: Temporal lobe epilepsy, histology, MRI, correlation, focal cortical dysplasia

www.manaraa.com

Acknowledgments

I would like to take this opportunity to thank all the people who have been instrumental in the completion of this thesis. I would like to express the deepest appreciation to my supervisors, Dr. Terry Peters and Dr. Ali Khan, without their continued support and endless patience this thesis would never have seen completion. I am immensely grateful for being provided with the opportunity to work on this project and it has been an honour to study under each of your guidance. Thank you also to the members of the VASST and Khan labs, it has been a pleasure working with all of you over the last several years. Thank you for sharing all of your knowledge and insights with me. I would like to thank my partner in life, Brandon, for his endless encouragement while working on my thesis. Without the love, tremendous patience and understanding I would not have been able to accomplish my goals. Finally, I would like to thank my wonderful parents and siblings, for their love, support and inspiration to follow my dreams. Your support and confidence in me has been essential to my success, and I am very appreciative for all you have done. Words cannot express my depth of gratitude to everyone that has supported me in this endeavor.

www.manaraa.com

Contents

www.manaraa.com

www.manaraa.com

www.manaraa.com

List of Figures

www.manaraa.com

www.manaraa.com

www.manaraa.com

List of Tables

www.manaraa.com

List of Acronyms

AEDs anti epileptic drugs

ATL anterior temporal lobectomy

CT computed tomography

CUSA Cavitron Ultrasonic Surgical Aspirator

DTI diffusion tensor imaging

EEG electroencephalograghy

FCD focal cortical dysplasia

fMRI functional Magnetic Resonance Imaging

GM gray matter

H&E Hematoxylin and Eosin

IHC ImmunoHistoChemistry

ILAE International League Against Epilepsy

MCD malformations of cortical development

MRI Magnetic Resonance Imaging

www.manaraa.com

NeuN Neuronal Nuclei

NMR Nuclear Magnetic Resonance

PET Positron Emission Tomography

ROI region of interest

SAH selective amygdalohippocampectomy

SPECT Single Photon Emission Computed Tomography

SVM support vector machine

TLE temporal lobe epilepsy

WM white matter

www.manaraa.com

Chapter 1

Introduction

1.1 Epilepsy

1.1.1 Introduction to Epilepsy

Epilepsy is a set of chronic neurological disorders that are characterized by abnormal neuronal activity causing recurrent seizures and affects approximately 65 million people worldwide [1]. Seizures are thought to be the consequence of an imbalance between inhibition and excitation, causing hyper-excitability of neuronal populations in the brain [2]. Seizures are categorized into two major groups based on onset, partial (focal) seizures, and generalized seizure, with partial seizures being confined to a small neuronal population in the brain and categorized as either simple or complex. Simple focal seizures result in exaggerated emotions or hallucinations, while complex focal seizures may result in unconsciousness. The onset of abnormal neuronal activity that begins in one structure of the brain and spreads throughout the entire brain is known as a generalized seizure and is categorized by the presence of convulsive movements.

Despite many advances in epilepsy research over the years and the vast availability of anti epileptic drugs (AEDs), the ability to eradicate seizures still remains highly limited. Approximately 25 to 30% of all epilepsy patients are resistant to treatment with AEDs

www.manaraa.com

[3]. Refractory epilepsy is associated with a high level of social stigmatization [4], decreased life expectancy [5], and other co-morbidities, ultimately placing a burden on patients' quality of life in addition to an economic burden [6, 7].

Temporal lobe epilepsy (TLE) is the most common cause of intractable refractory seizures and was described in detail by the International League Against Epilepsy (ILAE) in 1985 [8]. It is characterized by recurrent partial seizures that originate from the medial or lateral temporal lobe. Patients who suffer with medically intractable temporal lobe epilepsy are potential candidates for anterior temporal lobectomy (ATL) and it has proven to be a successful treatment, particularly in the presence of an associated lesion that is identifiable with neuroimaging techniques [9]. However, surgical treatment fails to provide a seizure-free outcome in 20 to 40% of TLE patients [10–13]. The reasons behind surgical failure vary from one patient to another, therefore the correct identification of the epileptogenic zone is important for preparing and planning the surgical resection [14].

1.1.2 Temporal Lobe Anatomy

The temporal lobe, seen in Figure 1.1, is one of four regions within the cerebral cortex and is associated with memory, speech perception and language comprehension in addition to visual, auditory and olfactory senses [15]. It's comprised of three cortices which consist of a six-layered neocortex, a three-layered archicortex that includes the hippocampus, the prepiriform area, the uncal semilunar gyrus, and the parahippocampus, the transitional region between the neocortex and the archicortex. The mesial structures of the temporal lobe consist of the hippocampus, amygdala, uncus, parahippocampal gyrus and entorhinal cortex, while the lateral temporal lobe comprises of the neocortex, which can be seen in Figure 1.2 [16].

www.manaraa.com

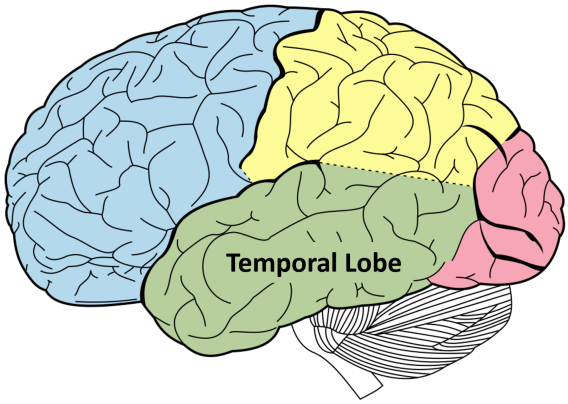

Figure 1.1: Position of the temporal lobe in the cerebral cortex. Modified from Henry Gray's anatomy: Figure 728. Licensed under Public domain via Wikimedia Commons.

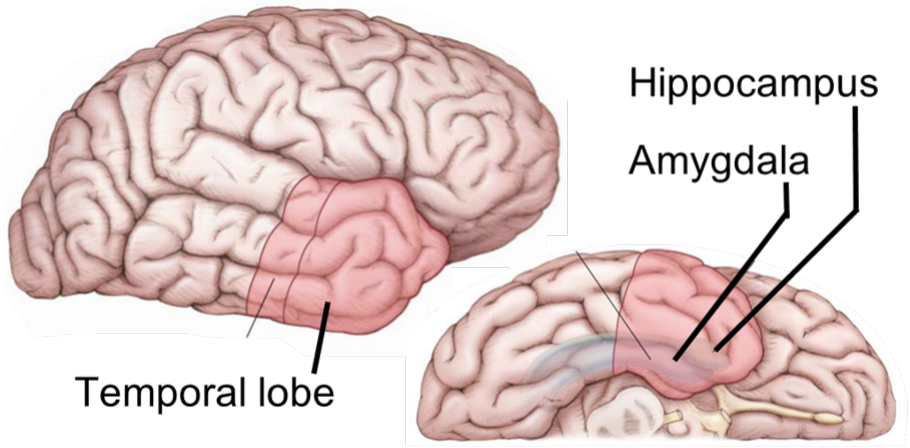

Figure 1.2: Structures of the temporal lobe demonstrating the outer temporal lobe neocortex along with the primary mesial structures underneath

www.manaraa.com

1.1.3 Neocortical Architecture

For most of the nineteenth century, there was much debate surrounding the organization of the nervous system. There were differing conclusions about the structure of the nervous system due to the poor resolution of the microscopes available at the time. It was Santiago Ramon y Cajal who suggested that the neuron was the functional unit of the nervous system [17].

There are several cell types in the cerebral cortex. The pyramidal cells are the primary cell type within layers III and V. Their most prominent feature is their pyramidal shape with an apical dendrite that extends to layer I. The thin axon that arises out from the base of the cell has long process that leaves the cortex and connects with other brain regions by extending through the white matter deep to the cortex. The granule cells are seen most prominently in layer IV and their axons remain within the cortex [18]. Neuroglia cells are not neurons but are supporting cells within the nervous system. The basic structure of a neuron, along with a neuroglial cell, can be seen in Figure 1.3.

The neocortex is the newest part of the cerebral cortex and is a distinguishing feature of the mammalian brain. The work of Brodmann in the early 20th century showed that the majority of the cerebral neocortex has six distinct cell layers in a lamina structure and covers most of the surface of the cerebral hemispheres [19]. Each cortical layer contains various types of neurons differing in shape, size and density. The six layers of this part of the cortex are numbered from the pial to the white matter, as seen in Figure 1.4. Layer I is the molecular layer, which contains very few cell bodies; layer II the external granular layer, containing small densely-packed pyramidal neurons; layer III, the external pyramidal layer, with mid-sized pyramidal neurons; layer IV, the internal granular layer, which is the most heavily populated layer containing granule cells; layer V, the internal pyramidal layer, contains the largest pyramidal neurons; and layer VI the multiform, or fusiform layer that contains a variety of neurons [18].

www.manaraa.com

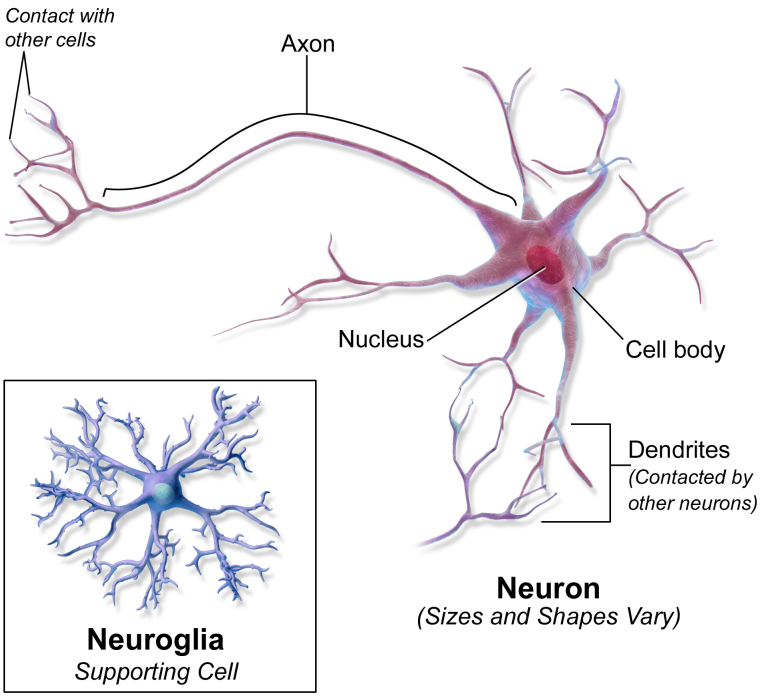

Figure 1.3: Basic structure of a neuron. Adapted from the Blausen Gallery, 2014. Wikiversity Journal of Medicine. Licensed under the Creative Commons Attribution 3.0 Unported license.

www.manaraa.com

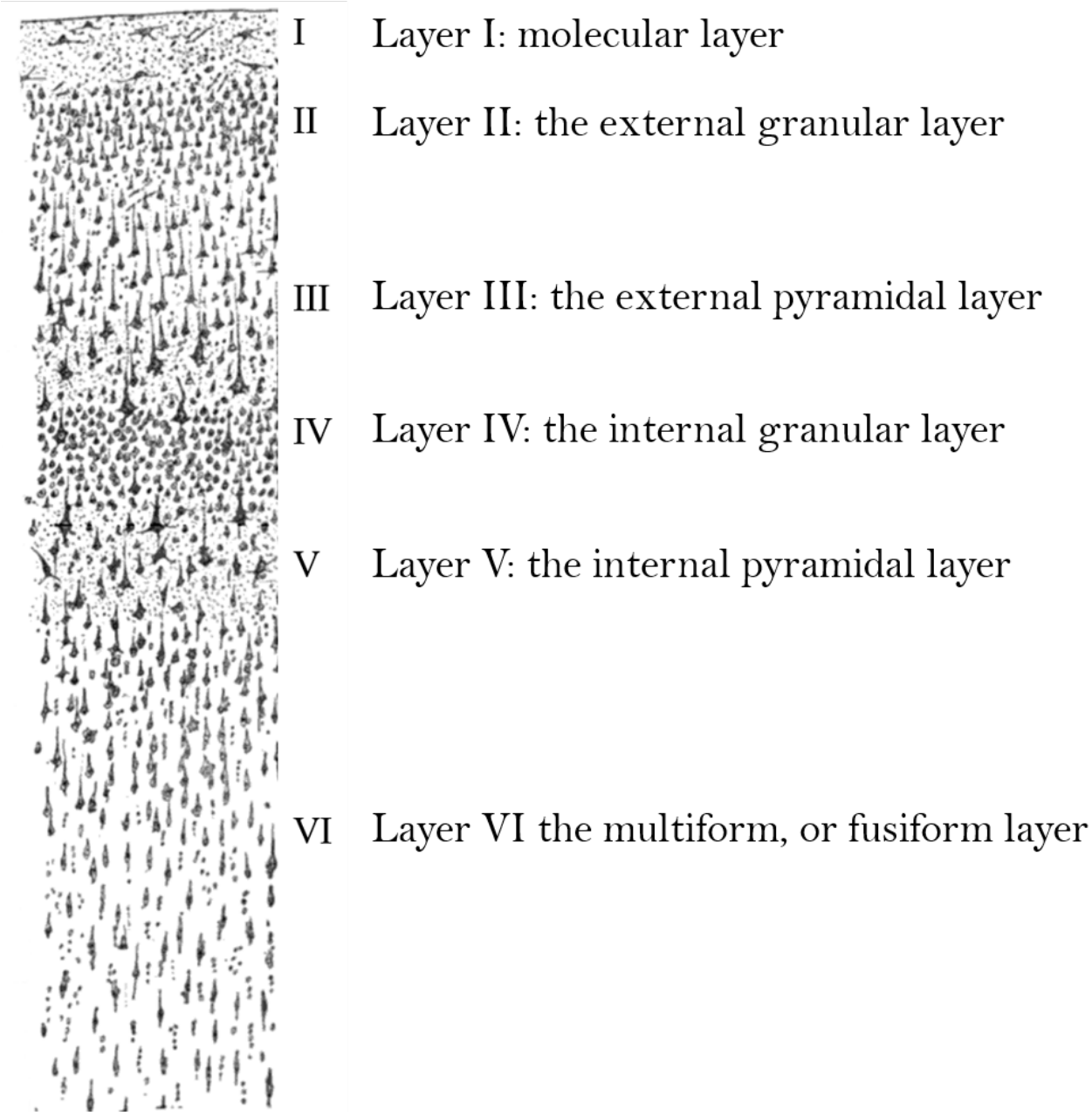

Figure 1.4: Cajal drawing showing cortical lamination in the human cerebral cortex. Modified from Santiago Ramon y Cajal's "Comparative study of the sensory areas of the human cortex", page 361. Licensed under Public domain via Wikimedia Commons.

www.manaraa.com

1.1.4 Pathology & Epileptogenicity of Temporal Lobe Epilepsy

Epileptogenesis

In order for the brain to function normally, neurons must maintain a highly interconnected and organized structure. Epileptogenesis is the sequence of events that converts a normal brain into one that supports seizures [2]. While there are many theories surrounding the current understanding of epileptogenesis, the changes that occur during epileptogenesis are poorly understood.

Cortical development, known as corticogenesis, is a highly complex and regulated process that starts from neurogenesis and proceeds in a series of precisely ordered steps of neuronal proliferation, neuronal migration and cortical organization [20]. Primitive neuronal cells originate in the neural tube and proliferate to become neuroblasts. The neuroblasts migrate along radial glial scaffolding and the cells organize into various layers establishing the cortical laminae structure, as described previously in Section 1.1.3. At this point the neurons undergo differentiation and synaptogensis, followed by myelination [21]. However, if this process is at all disrupted, abnormalities may form in the neocortical structure and individual cellular morphologies [22].

With recent advancements in neuroimaging, genetics and molecular biology there has been an increased awareness of cerebral cortex development and neuropathologic changes, especially in children [23]. Malformations of cortical development (MCD) are developmental brain lesions characterized by disruptions and abnormalities of the cerebral cortex and are inherently epileptogenic. These malformations consist of a wide group of disorders in which approximately 25% to 40% of intractable epilepsy is associated with MCD [24] and focal cortical dysplasia (FCD) is the most common presentation of MCD in epilepsy [25].

www.manaraa.com

Focal Cortical Dysplasia

Taylor first used the term FCD in 1971 to describe cortical abnormalities found in patients who presented with refractory partial epilepsy [26]. This term includes a wide range of lesions including disorganized cytoarchitecture, disruption of cortical lamination, disruption of radial organization and abnormal neuronal morphologies.To categorize these lesions, the ILAE recently introduced a three tier classification system that differentiates the various epileptogenic lesions known as FCDs.

FCD Type I is recognized as an isolated malformation with abnormal cortical layering, either showing radial abnormalities, characterized by microcolumns, in the cortical architecture (FCD Type Ia) or loss of the tangential architecture (FCD Type Ib), consisting of blurring between layers and the white matter, or complete loss of neuron populations. In addition, FCD Type Ic includes both lesion types, FCD Type Ia and FCD Type Ib, demonstrating both abnormal radial and tangential lamination patterns in the cortex.

FCD Type II is a malformation that presents altered cortical layering in addition to specific cytological abnormalities which may include FCD Type IIa, comprising the presence of dysmorphic neurons (neurons with significantly enlarged cell body and nucleus, malorientation or accumulation of neurofilament proteins) or FCD Type II presenting with dysmorphic neurons in addition to balloon cells. FCD Type III refers to architectural abnormalities that are associated with a lesion. These include lesions that are linked to hippocampal sclerosis (FCD Type IIIa), tumours (FCD Type IIIb), vascular malformations (FCD Type IIIc) and other principal lesions acquired during early life (FCD Type IIId) [27].

Although the proposed ILAE classification system for FCD exists, there is currently a lack of research towards providing objective, quantitative methods for characterization of cortical dysplasia in epilepsy. Recently, Muhlebner *et al* [28] systematically analyzed histological features in 52 epilepsy patients with evidence for FCD. They assessed measurements of cellular profiles , cortical thickness, heterotopic neurons in white matter

www.manaraa.com

and myelination and compared these measures to the patients' FCD assigned classification. Cellular profiles were based on measurements of the area of individual cell bodies and the diameter of neuronal cell bodies. Although their methodology presented a semi-quantitative approach in assessing morphological parameters for FCD subgroups, further work is required to better quantitatively characterize whole sections of cortical tissue.

Many previous studies demonstrating a quantitative analysis of neuropathology in epilepsy have taken the approach of assessing the field fraction of a given histology slide [29, 30]. Field fraction estimate is a commonly used measure representing the fraction of positively stained pixels in each field. However, field fraction provides limited information with respect to to the cortical architecture in epilepsy, thus further measures will allow for better analysis of architectural abnormalities. There have also been studies that have provided measures of neuron densities in both the cortex [31–33] and white matter [34, 35], however, since white matter neurons are so sparse, histological measurements in those cortical regions are limited and neuronal density alone is not a sufficiently specific method to encompass the entire spectrum of abnormalities in FCD. In addition, many of these studies involve only hippocampal histology or rely on user-intensive stereology methods [31, 35]. A study correlating cortical dysplasia with severity of seizures has shown that seizure frequency correlates well with the histologic grade [36]. Since resections in patients with FCD present a higher degree of complexity, there is a need for further quantitative and automated measures that can better apply the ILAE classification of FCD and assess abnormalities in cortical architecture.

1.1.5 Diagnostic Procedures

EEG

An electroencephalogram (EEG) detects electrical activity in the brain using electrodes attached to the scalp. Neurons communicate via electrical impulses and this activity

www.manaraa.com

shows up as waveforms on an EEG recording. In epilepsy diagnosis, abnormal waveforms often appear as spikes and wave patterns that can be used for lateralization and localization of the epileptic focus. Although beneficial in epilepsy monitoring, electroencephalograghy (EEG) alone is not sufficient for surgical planning or the determination of epileptogenic zones [37, 38].

Neuroimaging

Neuroimaging in epilepsy utilizes many different approaches and modalities. In particular, Magnetic Resonance Imaging (MRI) has had a high impact on clinical diagnosis and treatment in epilepsy, leading to a greater understanding of structural brain abnormalities associated with seizure activity [39].

MRI is a medical imaging technique that is most commonly used to visualize detailed internal structures of the body and makes use of the property of Nuclear Magnetic Resonance (NMR) to image nuclei of atoms inside the body. MRI is used over other medical imaging techniques, such as computed tomography (CT) or X-rays, since it provides contrast between the various soft tissues in the body. This makes this technique especially useful in imaging the brain and its varying tissues, particularly compared to CT that is considered to be unhelpful in cases of intractable epilepsy [39].

Conventional MRI, however, is inadequate for patients with refractory epilepsy, since FCD are often subtle and difficult to detect. The ILAE guideline for neuroimaging in patients with epilepsy recommend a dedicated MRI protocol for all patients with any new onset of seizure activity [40]. Additionally, the ILAE Commission on Neuroimaging recommends a specialized epilepsy MRI protocol in all patients with intractable epilepsy [41].

Other imaging modalities that are used in the evaluation of refractory epilepsy include functional Magnetic Resonance Imaging (fMRI), Single Photon Emission Computed Tomography (SPECT) and Positron Emission Tomography (PET) but the use of these

www.manaraa.com

imaging modalities for diagnostic purpose are currently outside the scope of this project.

1.1.6 Surgery

Surgical excision of the epileptogenic zone is the current standard of care for intractable focal epilepsy [42]. The first known surgical intervention of temporal lobe epilepsy was performed by Horsely in 1886 . He carried out surgical resections, removing lesions based on predicted seizure semiology [43]. Today, epilepsy patients are recommended for surgery when drug intervention or other therapies are ineffective in controlling seizures. In addition, there should be a reasonable likelihood that the seizure onset is focal and limited to one region of the brain. The process of recruiting surgical candidates involves a combination of evaluations including electrophysiological and neuroimaging instruments. The goal of surgery is to achieve seizure freedom and improve quality of life, by removal of the epileptogenic tissue, with minimal neurological or cognitive deficits to the patient. Temporal lobe resections are relatively safe procedures with mortality rates close to zero and continuously improving surgical techniques [44,45]. Currently there are two surgical methods that are used in the treatment of medically intractable TLE, the standard ATL or selective amygdalohippocampectomy (SAH).

Anterior Temporal Lobectomy

An ATL is the complete resection of the lateral temporal and mesial temporal structures of the brain. Standard general anaesthesia is most commonly used, however, some centres employ an awake craniotomy in order to perform intraoperative functional cortical mapping to avoid damage to critical regions.

The procedure first involves the *en bloc* removal of approximately 3-6 cm of the lateral temporal neocortex, which allows for better visualization of the mesial structures. The resection of the deeper mesial structures typically involves the removal of the hippocampus, amygdala, uncus, parahippocampal gyrus and entorhinal cortex [46]. The en bloc

www.manaraa.com

removal of these structures allows for pathologic examination of the specimen following surgery in comparison to an aspiration technique using a Cavitron Ultrasonic Surgical Aspirator (CUSA), which does not preserve the tissue for examination [47].

Selective Amygdalohippocampectomy

During SAH, the amygdala and hippocampus are targeted for removal, while the surrounding structures, including the neocortex of the temporal lobe, are preserved. This procedure is considered to be minimally invasive and is typically used for patients with clear evidence of mesial temporal lobe seizure foci without lateral temporal neocortex indications.

During this procedure the patient is positioned similarly to the ATL but a smaller linear or curvilinear incision is used [46]. Typically, the mesial resection of this procedure is performed using an ultrasonic aspirator for much of the tissue, which does not allow for later pathologic examination, however, en bloc removal of the hippocampal structure is possible [46].

Surgical Risks and Outcomes

Surgical complications from temporal lobe resective procedures are relatively uncommon [46]. However, the most commonly associated neuropsychological risks involved with temporal lobe surgery are memory loss, visual field deficits, speech difficulties and emotional or personality changes. Surgical complications involve wound infection, postoperative hydrocephalus, meningitis, and hematomas [44]. The mortality following surgery for TLE is rare [45] and has been noted to be between 0% and 3.5% across several studies [44]. Accurate knowledge of potential risks and complications is important for preventing them and many of the factors surrounding surgical complications can be avoided a thorough medical screening and patient history [48].

Following temporal lobe surgery, approximately one-third of patients continue to ex-

www.manaraa.com

perience seizures [49]. Surgical treatment presents many challenges in locating the epileptogenic focus and thus not all patients become seizure-free following surgery. For this reason, further research is necessary to ensure seizure freedom in a higher percentage of epilepsy patients. The most important predictor of a successful resection is the complete resection of the epileptogenic zone as detected by MRI prior to the surgery.

1.1.7 MRI-Histology Correlation

The key to identifying epileptogenic abnormalities in epilepsy patients relies heavily on a multi-parametric approach. Advances in MR imaging techniques can lead to improved localization of the epileptogenic zone and may be validated by correlating MRI with histology of the excised cortical tissue following surgery [32,50–53]. As mentioned previously in Section 1.1.4, malformations, that are present in mildly dysplastic cortical tissue, are often subtle and difficult to quantify. Using quantitative analysis techniques, the various pathologies in epilepsy lesions can be characterized into digital histology signatures, with the expectation that abnormal tissue would have a different signature than that of a normal tissue sample, as seen in Figure 1.5.

To perform a correlation study between MR images and histology images, an accurate registration must first be performed, as demonstrated in Figure 1.6. Thus far the work by Goubran [54,55] has demonstrated a robust registration pipeline that allows for an accurate spatial correspondence of histology to ex-vivo MRI in addition to the registration between histology and in-vivo MRI. This process can present many challenges, since often histological tissue is not available following surgery in the case of aspiration techniques, and available tissue may be deformed from surgical resection or may present with distortions from the various steps involved with histological tissue processing.

Currently, there is a lack of research in the relationship between neuroimaging and histopathology. A 2011 surgical study demonstrated that dysplastic lesions are missed in clinical MRI in up to 87% of cases with Type I FCD and 33% Type II FCD [56]. These

www.manaraa.com

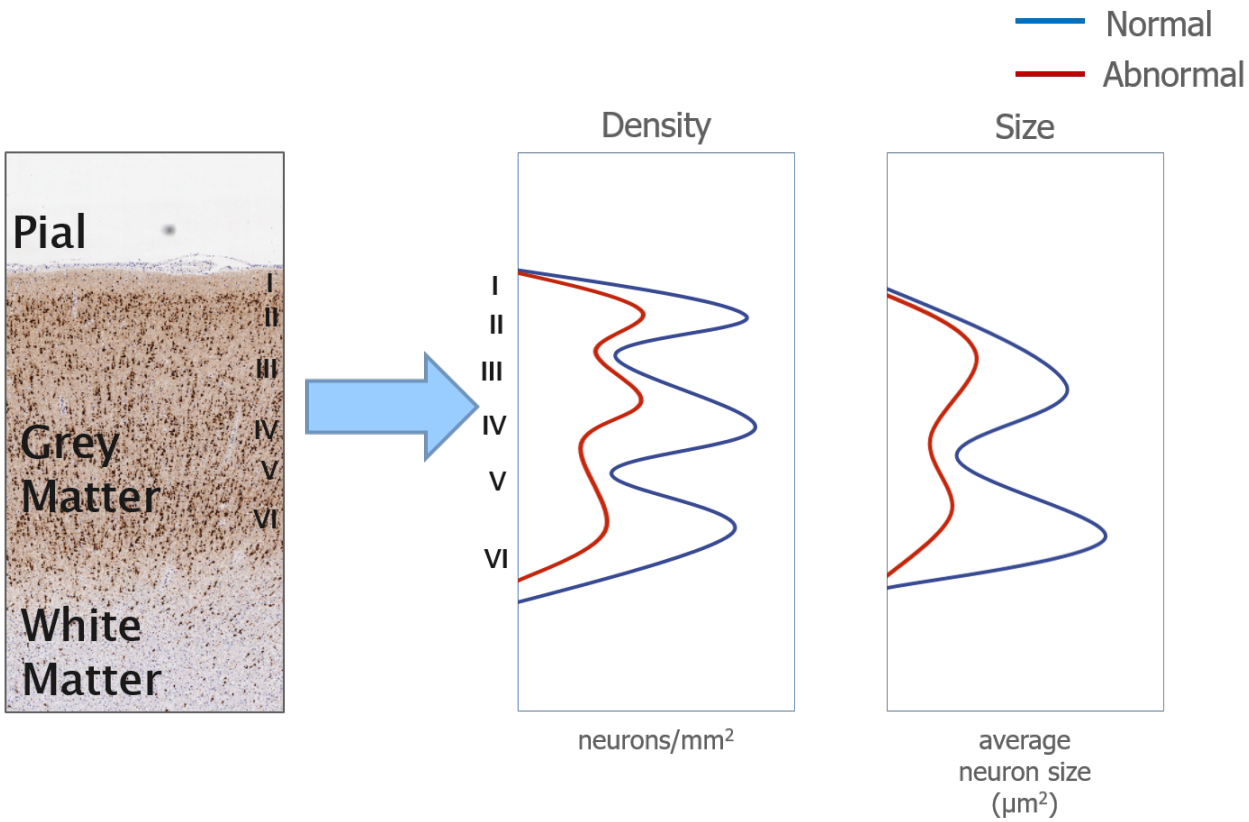

Figure 1.5: Digital histology signature

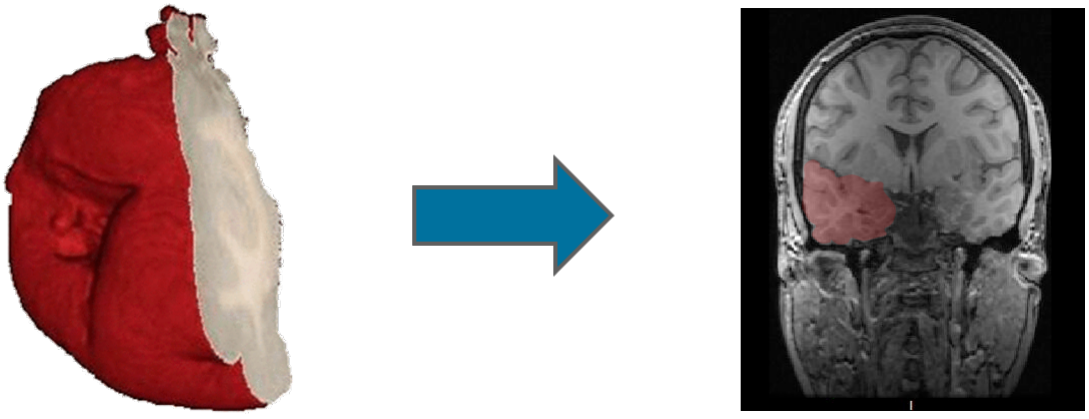

Figure 1.6: MRI and Histology Registration

www.manaraa.com

poor detection rates are related to the limitations in current imaging resolutions in addition to a lack of quantitative characterization and analysis of FCD lesions. Additionally, a study correlating MRI [32] to neuronal size and density found significant correlation but further measures of cortical abnormality are necessary to accurately predict and identify epileptogenic zones. These findings motivate the need for further MRI-histology in-vivo correlation studies that are usable in pre-operative visualization and planning. Predictive in-vivo histology maps would allow for the identification of epileptogenic zones prior to surgery, thus improving surgical resection outcomes.

1.2 Histopathology

Histopathology is a component of pathology that refers to the examination of tissue samples in order to study disease. The histological evaluation of tissue is critical to many applications, and the quantification and characterization of specimens aids in specific diagnoses.

1.2.1 Tissue Preparation

The process of histopathological examination begins with the acquisition of tissue samples via biopsy or surgery. Before the sample can be examined by the pathologist, it must be prepared via the following four primary steps:

1. Fixation,
2. Embedding,
3. Sectioning, and
4. Staining,

www.manaraa.com

Fixation

The tissue is removed from the body and placed in a fixative in order to both preserve and stabilize the tissue. Chemical fixatives work to preserve the tissue from degradation and also help to maintain the structure of both the cells and other components of the tissue. Standard fixation often uses a solution of formaldehyde, which is buffered and osmotically balanced to minimize shrinkage, swelling, and other damage of the tissue resulting in image artifacts.

Embedding

The fixation is followed by embedding, in which the water content of the tissue is removed with the use of solvents such as alcohol and xylene, and replaced by a solidifying ingredient such as paraffin wax.

Sectioning

Paraffin blocks are placed onto the microtome for slicing. Sections for routine light microscopy are typically between 5 µm and 10 µmin thickness. Although sections can be cut in a number of directions, the standard method for pathological evaluation of tissue is a cut made perpendicular to the tissue surface. The sections are then mounted onto slides for analysis.

Staining

Since many tissues are colourless and transparent, structural and cellular details are not visible unless the tissue is first stained to obtain contrast. Before staining, paraffin embedded sections must be rehydrated in a reverse process described in embedding. Hematoxylin and eosin (H&E stain) is the most common stain used in the fields of histology and histopathology. First, hematoxylin stains the nuclei blue due to it's affinity to nucleic acids in the cell nucleus while eosin stains the cytoplasm pink. Immunohis-

www.manaraa.com

tochemistry is the process of using antibodies to specifically visualize proteins within a tissue sample.

1.2.2 Image Artifacts

Artifacts can result from each step in tissue processing and caution must be taken to minimize these artifacts as much as possible. Tissue processing commonly leads to various changes in the tissue specimen such as tissue shrinkage, inconsistent color changes, and alterations of the cellular components and anatomical structures in the tissue. Various deformations must be considered and accounted for in tissue analysis. Colour constancy can cause particular issues for computer-aided analysis and is hard to control during the staining process and pooling of the stain naturally occurs.

Ideal tissue preparation preserves cells in a form that most closely represents the tissue *in-vivo*. However, this is not always practical within a clinical setting since in most post mortem samples, cells have been deteriorating for several hours before fixation is possible. Since the advent of digital histology and image analysis, this has become even more of a problem since many automated image analysis algorithms have difficulty handling image artifacts [57]. Therefore, colour normalization and other image processing techniques may be required before analysis.

1.2.3 Digitization

In general, the procedure for automatic analysis of histology images typically begins with the acquisition of the digital images. An image captured by a sensor is considered to be a continuous function of two coordinates, x and y, within a plane. The digitization process moves this function into a discrete matrix of M rows and N columns, with each cell pertaining to the location of a pixel within the image. The two-dimensional digital image is represented as a three-dimensional array in which x and y coordinates describe the pixel position, while the z coordinate contains the pixel's intensity value. In a greyscale

www.manaraa.com

image the z coordinate contains a single intensity value while in a colour image further information is required thus a vector of intensity values represents the colour components.

1.3 Digital Histology Processing

The introduction of digital histology has allowed for the simplification of many aspects of image processing involved in histology image analysis. However, manual interpretation of tissue slides is still highly labour intensive and is a highly visual and subjective task [58]. For this reason, there are many inconsistencies and risks for human error in image analysis. Digital image analysis is an alternative approach to manual interpretation by providing automatic, fast and reproducible results. The procedure for automatic analysis of digital histology images most commonly involves image segmentation, feature extraction, and the application of various learning algorithms [59, 60].

1.3.1 Colour Space

Colour represents a significant source of information within an image. A histological digital image can be represented with various colour spaces with the most common representation in a digital image being the RGB model that refers to the red, green and blue colour channels of an image. This colour model can be represented as a three dimensional colour space as seen in figure 1.7, where each pixel is represented as a three-dimensional vector (R,G,B) pertaining to the pixel's intensity of each colour component.

Another common colour model, seen in Figure 1.8, is HSV, a transformation of the RGB colour space in which a colour is decoupled from intensity and is represented by its Hue, Saturation and Value. The hue (H) refers to the colour, saturation (S) is a measure of white within the colour and value (V) describes the brightness of the pixel.

www.manaraa.com

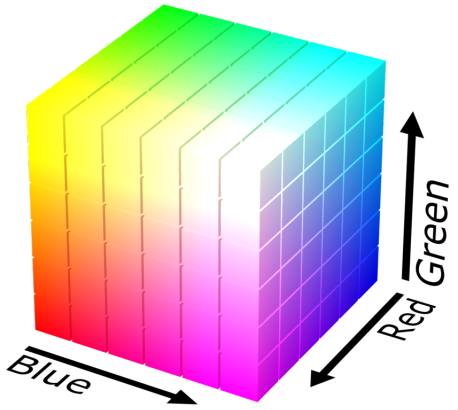

Figure 1.7: RGB colour model mapped to a cube. Licensed under the Creative Commons Attribution License.

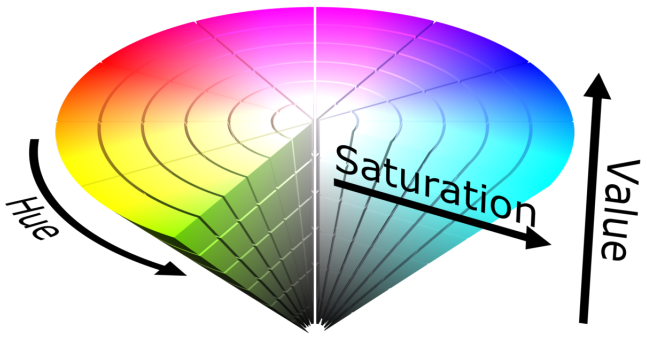

Figure 1.8: HSV Colour Model represented as a single cone. Licensed under the Creative Commons Attribution License.

www.manaraa.com

1.3.2 Colour Deconvolution

In pathology, image processing algorithms often use colour for detection of specific proteins and to separate various cellular structures within a tissue sample. In histologic staining, in most cases tissue samples are stained with several colours. The goal of colour deconvolution is to separate the image into three colour channels, indicating the distribution of the staining. This method is based on the absorption characteristics of an individual stain. One of the most common methods of colour deconvolution is based on the transformation of an RGB image to a single colour channel and was proposed by Ruifrok and Johnston [61]. The technique uses the principles of the Lambert-Beer law where the intensity of light over a thickness, x, in the sample is:

$$I_x = I_0 e^{-\alpha c x} \tag{1.1}$$

where I_0 is the incident intensity; α is the absorption factor of the stain; c is the concentration of the stain and the product $\alpha c x$ is the optical density.

This equation can be used to model the image formation process in bright field microscopy. Since images are captured by three channels (red, green and blue), each having known optical densities, the concentrations of stains can be determined for each pixel location which can be used to obtain single stain images. To perform the stain separation, an orthonormal transform of the RGB image is performed, providing information regarding the stain's concentration. This transformation must be both orthogonal and normalized to allow for specific staining information and a balanced representation of the absorption factor, α, for each stain. The normalized OD matrix, M, for an example case of hematoxylin, eosin and DAB can be seen in Figure 1.9 [61].

www.manaraa.com

$$M = \left(\begin{array}{ccc|c} R & G & B & \\ 0.65 & 0.704 & 0.286 & \text{Haematoxylin} \\ 0.072 & 0.99 & 0.105 & \text{Eosin} \\ 0.268 & 0.57 & 0.776 & \text{DAB} \end{array} \right)$$

Figure 1.9: Normalized Optical Density matrix for Haematoxylin, Eosin and DAB

1.3.3 Image Segmentation

Segmentation is the process of dividing an image into meaningful regions or categories and is one of the most important tools used in image analysis. Meaningful regions are separated from the background and from each other using a variety of segmentation techniques, including region-based and edge-based methods. The use of further image analysis such as feature extraction and object classification, depend on the result of the segmentation and therefore it is necessary for segmentations to be as accurate as possible.

Thresholding

Image thresholding techniques are simple, well known and intuitive. The purpose of a thresholding procedure is to determine an intensity value, called the threshold, which separates the image into desired regions within an image. The segmentation is then achieved by grouping all pixels with intensity greater than the threshold into one subset, and all other pixels into a separate set. These global methods are effective when the intensity levels of the objects of interest fall entirely outside the range of background intensity levels. However, since spatial information of the image is ignored, blurred region boundaries can be problematic.

www.manaraa.com

Watershed Segmentation

The watershed transformation algorithm was formulated by Beucher and Lantujoule and is one of the oldest segmentation techniques [62]. The watershed transformation is useful since it provides a means to separate overlapping objects and allows for a lower computation time and more accurate result compared to other existing segmentation methods [63]. Unfortunately, using a standard morphological watershed algorithm on an image often results in over-segmentation due to the presence of many local minima. An over-segmentation is the process by which objects within an image are segmented from the background but are themselves segmented, resulting in fractured image components. To combat this problem, there have been many proposed solutions in literature to decrease over-segmentation in watershed algorithms by reducing the number of minima [64, 65]. A major enhancement of the watershed transformation, found to be particularly useful in cell segmentation, consists in 'flooding' the topographic surface using a set of defined markers and is known as the marker-based watershed algorithm [66]. In a marker-based watershed segmentation both foreground and background markers are indicated and be determined using a number of techniques such as edge detection, morphological filtering and thresholding.

1.3.4 Histology Image Analysis

Quantitative measurement is usually the ultimate goal of histological image analysis. Once an image has been segmented into meaningful regions and objects, various measurements can be made on these objects. Perhaps the most common image representation for histology images is the feature vector. Feature vectors can be built up for each pixel, for regions, sub-blocks or for the complete image. The dimensionality of the feature vector is the most important aspect to be considered, in order to make sense in the way they will be interpreted and processed.

www.manaraa.com

An alternative image representation is to preserve the descriptors for all objects in the image. Objects in histology images can be cells, nuclei, glands or simply sub-blocks. For each of those objects, a feature vector is constructed and all these vectors are organized in a table or matrix. Note that the number of objects from image to image may be different, while the length of the feature vector is fixed.

1.4 Thesis Objectives

The overall goals of this thesis can be defined as follows:

1. To develop and validate a segmentation process to individually delineate neurons in histopathology specimens.

2. To investigate histological image features that are associated with epilepsy lesions and create a means of classifying regions of epileptic tissue.

3. To relate findings to clinical applications relevant to intractable TLE.

1.5 Thesis Outline

The following chapters in this thesis indicate how these objectives were achieved.

1.5.1 Chapter 2 - Neuron Segmentation, Feature Extraction and Clinical Applications

The focus of this chapter is to develop an automated segmentation and analysis pipeline that can assess regions of neuronal tissue. It presents methodology and validation for using specific features associated with FCD. A quantitative cortical architecture histology analysis is also applied to clinical data and the developed algorithms are assessed for clinical relevance in relation to FCD in temporal lobe epilepsy.

www.manaraa.com

1.5.2 Chapter 3 - Conclusions

This chapter will detail the conclusions and impact of the research included in this thesis, along with a discussion of limitations within the work. Future directions of the project will also be discussed.

www.manaraa.com

Bibliography

[1] E. Foundation, "About Epilepsy: The Basics," 2015.

[2] H. E. Scharfman, "The neurobiology of epilepsy," *Current neurology and neuroscience reports*, vol. 7, no. 4, pp. 348–354, 2007.

[3] A. J. Wood, M. A. Dichter, and M. J. Brodie, "Drug therapy: New antiepileptic drugs," *The New England journal of medicine*, vol. 334, pp. 1583–1590, June 1996.

[4] A. Jacoby and J. K. Austin, "Social stigma for adults and children with epilepsy," *Epilepsia*, vol. 48 Suppl 9, pp. 6–9, 2007.

[5] A. Gaitatzis, A. L. Johnson, D. W. Chadwick, S. D. Shorvon, and J. W. Sander, "Life expectancy in people with newly diagnosed epilepsy," *Brain*, vol. 127, pp. 2427–2432, Nov. 2004.

[6] A. Gaitatzis, S. M. Sisodiya, and J. W. Sander, "The somatic comorbidity of epilepsy: A weighty but often unrecognized burden," *Epilepsia*, vol. 53, pp. 1282–1293, Aug. 2012.

[7] E. I. Viteva and Z. I. Zahariev, "Depressivity, anxiety and quality of life in patients with refractory epilepsy," *Folia Medica*, vol. 51, pp. 42–49, Mar. 2009.

[8] C. on Classification and Terminology of the International League Against Epilepsy, "Proposal for Classification of Epilepsies and Epileptic Syndromes," *Epilepsia*, vol. 26, no. 3, pp. 268–278, 1985.

[9] Z. Yin, H. Kang, W. Wu, M. Wang, and S. Zhu, "Do neuroimaging results impact prognosis of epilepsy surgery? A meta-analysis," *Journal of Huazhong University of Science and Technology [Medical Sciences]*, vol. 33, no. 2, pp. 159–165, 2013.

www.manaraa.com

[10] L. Tassi, N. Colombo, R. Garbelli, S. Francione, G. L. Russo, R. Mai, F. Cardinale, M. Cossu, A. Ferrario, C. Galli, M. Bramerio, A. Citterio, and R. Spreafico, "Focal cortical dysplasia: neuropathological subtypes, EEG, neuroimaging and surgical outcome," *Brain*, vol. 125, no. 8, pp. 1719–1732, 2002.

[11] K. Radhakrishnan, E. L. So, P. L. Silbert, J. J. C. R, G. D. Cascino, F. W. Sharbrough, and P. C. O'Brien, "Predictors of outcome of anterior temporal lobectomy for intractable epilepsy: a multivariate study," *Neurology*, vol. 51, no. 2, pp. 465–471, 1998.

[12] L. E. Jeha, R. A. Prayson, Y. Comair, R. O'Brien, J. Bulacio, A. Gupta, H. O. Lders, I. M. Najm, W. E. Bingaman, F. Khandwala, P. Widdess-Walsh, H. H. Morris, D. S. Dinner, D. Nair, and N. Foldvary-Schaeffer, "Predictors of outcome after temporal lobectomy for the treatment of intractable epilepsy," *Neurology*, vol. 66, no. 12, pp. 1938–1940, 2006.

[13] A. M. McIntosh, R. M. Kalnins, L. A. Mitchell, G. C. A. Fabinyi, R. S. Briellmann, and S. F. Berkovic, "Temporal lobectomy: long-term seizure outcome, late recurrence and risks for seizure recurrence," *Brain : a journal of neurology*, vol. 127, no. Pt 9, pp. 2018–2030, 2004.

[14] A. Harroud, A. Bouthillier, A. G. Weil, and D. K. Nguyen, "Temporal Lobe Epilepsy Surgery Failures: A Review," *Epilepsy Research and Treatment*, vol. 2012, p. e201651, Apr. 2012.

[15] J. A. Kiernan, "Anatomy of the Temporal Lobe," *Epilepsy Research and Treatment*, vol. 2012, p. e176157, Mar. 2012.

[16] J. A. Kiernan and M. L. Barr, *Barr's the Human Nervous System: An Anatomical Viewpoint*. Lippincott Williams & Wilkins, 2009. Google-Books-ID: 65outatc1woC.

www.manaraa.com

[17] S. R. y. Cajal, *Histology of the nervous system of man and vertebrates*. Oxford University Press, 1995.

[18] S. K. Leong, *An Introduction to the Human Nervous System*. NUS Press, 1986.

[19] K. Brodmann and L. J. Garey, *Brodmann's: Localisation in the Cerebral Cortex*. Springer Science & Business Media, Feb. 2007.

[20] A. R. Kriegstein, "Determination of the cellular phenotype and the fundamental organization of cortical layering: an overview," in *The Cortical Neuron* (M. Gutnick and I. Mody, eds.), pp. 193–196, Oxford University Press, 1995.

[21] P. Rakic, "Specification of Cerebral Cortical Areas," *Science*, vol. 241, pp. 170–176, July 1988.

[22] A. C. Flint and A. R. Kriegstein, "Mechanisms underlying neuronal migration disorders and epilepsy. [Editorial]," *Current Opinion in Neurology*, vol. 10, pp. 92–97, Apr. 1997.

[23] A. J. Barkovich, R. Guerrini, R. I. Kuzniecky, G. D. Jackson, and W. B. Dobyns, "A developmental and genetic classification for malformations of cortical development: update 2012," *Brain: A Journal of Neurology*, vol. 135, pp. 1348–1369, May 2012.

[24] R. J. Leventer, R. Guerrini, and W. B. Dobyns, "Malformations of cortical development and epilepsy," *Dialogues in Clinical Neuroscience*, vol. 10, no. 1, pp. 47–62, 2008.

[25] S. M. Sisodiya, "Surgery for malformations of cortical development causing epilepsy," *Brain*, vol. 123, pp. 1075–1091, June 2000.

[26] D. C. Taylor, M. A. Falconer, C. J. Bruton, and J. A. N. Corsellis, "Focal dysplasia of the cerebral cortex in epilepsy," *Journal of Neurology, Neurosurgery & Psychiatry*, vol. 34, no. 4, pp. 369–387, 1971.

www.manaraa.com

[27] I. Blumcke, M. Thom, E. Aronica, D. D. Armstrong, H. V. Vinters, A. Palmini, T. S. Jacques, G. Avanzini, A. J. Barkovich, and G. Battaglia, "The clinicopathologic spectrum of focal cortical dysplasias: A consensus classification proposed by an ad hoc Task Force of the ILAE Diagnostic Methods Commission1," *Epilepsia*, vol. 52, no. 1, pp. 158–174, 2011.

[28] A. Muhlebner, R. Coras, K. Kobow, M. Feucht, T. Czech, H. Stefan, D. Weigel, M. Buchfelder, H. Holthausen, and T. Pieper, "Neuropathologic measurements in focal cortical dysplasias: validation of the ILAE 2011 classification system and diagnostic implications for MRI," *Acta Neuropathologica*, vol. 123, no. 2, pp. 259–272, 2012.

[29] F. Blanc, L. Martinian, I. Liagkouras, C. Catarino, S. M. Sisodiya, and M. Thom, "Investigation of widespread neocortical pathology associated with hippocampal sclerosis in epilepsy: A postmortem study," *Epilepsia*, vol. 52, pp. 10–21, Jan. 2011.

[30] S. H. Eriksson, S. L. Free, M. Thom, L. Martinian, M. R. Symms, T. M. Salmenpera, A. W. McEvoy, W. Harkness, J. S. Duncan, and S. M. Sisodiya, "Correlation of quantitative MRI and neuropathology in epilepsy surgical resection specimens and T2 correlates with neuronal tissue in gray matter," *NeuroImage*, vol. 37, no. 1, pp. 48–55, 2007.

[31] B. Sinjab, L. Martinian, S. M. Sisodiya, and M. Thom, "Regional thalamic neuropathology in patients with hippocampal sclerosis and epilepsy: a postmortem study," *Epilepsia*, vol. 54, pp. 2125–2133, Dec. 2013.

[32] M. Goubran, R. R. Hammond, S. de Ribaupierre, J. G. Burneo, S. Mirsattari, D. A. Steven, A. G. Parrent, T. M. Peters, and A. R. Khan, "Magnetic resonance imaging and histology correlation in the neocortex in temporal lobe epilepsy," *Annals of Neurology*, vol. 77, pp. 237–250, Feb. 2015.

www.manaraa.com

[33] S. Bothwell, G. E. Meredith, J. Phillips, H. Staunton, C. Doherty, E. Grigorenko, S. Glazier, S. A. Deadwyler, C. A. O'Donovan, and M. Farrell, "Neuronal Hypertrophy in the Neocortex of Patients with Temporal Lobe Epilepsy," *The Journal of Neuroscience*, vol. 21, pp. 4789–4800, July 2001.

[34] S. H. Eriksson, S. L. Free, M. Thom, L. Martinian, and S. M. Sisodiya, "Methodological aspects of 3d and automated 2d analyses of white matter neuronal density in temporal lobe epilepsy," *Neuropathology and applied neurobiology*, vol. 32, no. 3, pp. 260–270, 2006.

[35] J. Y. W. Liu, M. Ellis, H. Brooke-Ball, J. de Tisi, S. H. Eriksson, S. Brandner, S. M. Sisodiya, and M. Thom, "High-throughput, automated quantification of white matter neurons in mild malformation of cortical development in epilepsy," *Acta Neuropathologica Communications*, vol. 2, p. 72, 2014.

[36] H. Miyata, T. Hori, and H. V. Vinters, "Surgical pathology of epilepsy-associated non-neoplastic cerebral lesions: A brief introduction with special reference to hippocampal sclerosis and focal cortical dysplasia," *Neuropathology*, vol. 33, pp. 442–458, Aug. 2013.

[37] E. H. Bertram, "Electrophysiology in epilepsy surgery: Roles and limitations," *Annals of Indian Academy of Neurology*, vol. 17, pp. S40–S44, Mar. 2014.

[38] E. B. Bromfield, J. E. Cavazos, and J. I. Sirven, *Epilepsy Surgery*. American Epilepsy Society, 2006.

[39] V. Gupta and R. A. Bronen, "MRI: Overview of MR Teachniques For Epilepsy," in *Neuroimaging in Epilepsy* (H. T. Chugani, ed.), Oxford University Press, 2011.

[40] C. on Neuroimaging of the International League Against Epilepsy, "Recommendations for Neuroimaging of Patients with Epilepsy," *Epilepsia*, vol. 38, pp. 1255–1256, Nov. 1997.

www.manaraa.com

[41] C. on Neuroimaging of the International League Against Epilepsy, "Guidelines for Neuroimaging Evaluation of Patients with Uncontrolled Epilepsy Considered for Surgery," *Epilepsia*, vol. 39, pp. 1375–1376, Dec. 1998.

[42] M. Thom, G. W. Mathern, J. H. Cross, and E. H. Bertram, "Mesial Temporal Lobe Epilepsy: How do we improve surgical outcome?," *Annals of neurology*, vol. 68, pp. 424–434, Oct. 2010.

[43] V. Horsley, "Brain-Surgery," *The British Medical Journal*, vol. 2, no. 1345, pp. 670–675, 1886.

[44] I. Georgiadis, E. Z. Kapsalaki, and K. N. Fountas, "Temporal Lobe Resective Surgery for Medically Intractable Epilepsy: A Review of Complications and Side Effects," *Epilepsy Research and Treatment*, vol. 2013, 2013.

[45] B. Fisch, "Anterior Temporal Lobectomy How Safe Is It?," *Epilepsy Currents*, vol. 11, no. 6, pp. 186–188, 2011.

[46] F. Al-Otaibi, S. S. Baeesa, A. G. Parrent, J. P. Girvin, and D. Steven, "Surgical techniques for the treatment of temporal lobe epilepsy," *Epilepsy research and treatment*, vol. 2012, pp. 374848–13, 2012.

[47] W. M. Burnham, P. L. Carlen, and P. A. Hwang, *Intractable Seizures: Diagnosis, Treatment, and Prevention*. Springer Science & Business Media, Dec. 2012. Google-Books-ID: zSQBCAAAQBAJ.

[48] A. Mansouri, A. Fallah, T. A. Valiante, A. Mansouri, A. Fallah, and T. A. Valiante, "Determining Surgical Candidacy in Temporal Lobe Epilepsy, Determining Surgical Candidacy in Temporal Lobe Epilepsy," *Epilepsy Research and Treatment, Epilepsy Research and Treatment*, vol. 2012, 2012, p. e706917, Feb. 2012.

www.manaraa.com

[49] J. J. Engel, "Surgery for Seizures," *New England Journal of Medicine*, vol. 334, pp. 647–653, Mar. 1996.

[50] Z. I. Wang, A. V. Alexopoulos, S. E. Jones, Z. Jaisani, I. M. Najm, and R. A. Prayson, "The pathology of magnetic-resonance-imaging-negative epilepsy," *Modern Pathology*, vol. 26, pp. 1051–1058, Aug. 2013.

[51] P. Widdess-Walsh, C. Kellinghaus, L. Jeha, P. Kotagal, R. Prayson, W. Bingaman, and I. M. Najm, "Electro-clinical and imaging characteristics of focal cortical dysplasia: Correlation with pathological subtypes," *Epilepsy Research*, vol. 67, pp. 25–33, Oct. 2005.

[52] H. Urbach, D. Binder, M. v. Lehe, M. Podlogar, C. G. Bien, A. Becker, J. Schramm, T. Kral, and H. Clusmann, "Correlation of MRI and histopathology in epileptogenic parietal and occipital lobe lesions," *Seizure - European Journal of Epilepsy*, vol. 16, pp. 608–614, Oct. 2007.

[53] E. Wyllie, G. D. Cascino, B. E. Gidal, and H. P. Goodkin, *Wyllie's Treatment of Epilepsy: Principles and Practice*. Lippincott Williams & Wilkins, Feb. 2012. Google-Books-ID: j9t6Qg0kkuUC.

[54] M. Goubran, C. Crukley, S. d. Ribaupierre, T. M. Peters, and A. R. Khan, "Image registration of ex-vivo MRI to sparsely sectioned histology of hippocampal and neocortical temporal lobe specimens," *NeuroImage*, vol. 83, no. 0, pp. 770–781, 2013.

[55] M. Goubran, S. de Ribaupierre, R. R. Hammond, C. Currie, J. G. Burneo, A. G. Parrent, T. M. Peters, and A. R. Khan, "Registration of in-vivo to ex-vivo MRI of surgically resected specimens: A pipeline for histology to in-vivo registration," *Journal of Neuroscience Methods*, vol. 241, pp. 53–65, Feb. 2015.

www.manaraa.com

[56] A. Bernasconi, N. Bernasconi, B. C. Bernhardt, and D. Schrader, "Advances in MRI for 'cryptogenic' epilepsies," *Nature Reviews Neurology*, vol. 7, pp. 99–108, Feb. 2011.

[57] S. W. O'Driscoll, R. G. Marx, D. E. Beaton, Y. Miura, S. H. Gallay, and J. S. Fitzsimmons, "Validation of a Simple Histological-Histochemical Cartilage Scoring System," *Tissue Engineering*, vol. 7, pp. 313–320, June 2001.

[58] A. E. Rizzardi, A. T. Johnson, R. I. Vogel, S. E. Pambuccian, J. Henriksen, A. P. Skubitz, G. J. Metzger, and S. C. Schmechel, "Quantitative comparison of immunohistochemical staining measured by digital image analysis versus pathologist visual scoring," *Diagnostic Pathology*, vol. 7, p. 42, 2012.

[59] L. Mulrane, E. Rexhepaj, S. Penney, J. J. Callanan, and W. M. Gallagher, "Automated image analysis in histopathology: a valuable tool in medical diagnostics," *Expert Review of Molecular Diagnostics*, vol. 8, pp. 707–725, Nov. 2008.

[60] D. Pham, C. Xu, and J. Prince, "Current Methods in Medical Image Segmentation," *Annual Review of Biomedical Engineering*, vol. 2, no. 1, pp. 315–337, 2000.

[61] A. C. Ruifrok and D. A. Johnston, "Quantification of histochemical staining by color deconvolution," *Anal Quant Cytol Histol*, vol. 23, no. 4, pp. 291–299, 2001.

[62] Beucher, S. and Lantujoul, C., "Use of Watersheds in Contour Detection," *In International Workshop on Image Processing: Real-time Edge and Motion Detection/Estimation*, vol. 132, 1979.

[63] F. Ajala, O. Fenwa, and M. Aku, "A comparative analysis of watershed and edge based segmentation of red blood cells," *International Journal of Medicine and Biomedical Research*, vol. 4, no. 1, pp. 1–7, 2015.

www.manaraa.com

[64] H. P. Ng, S. H. Ong, K. W. C. Foong, P. S. Goh, and W. L. Nowinski, "Medical Image Segmentation Using K-Means Clustering and Improved Watershed Algorithm," in *2006 IEEE Southwest Symposium on Image Analysis and Interpretation*, pp. 61–65, 2006.

[65] V. Grau, A. U. J. Mewes, M. Alcaniz, R. Kikinis, and S. K. Warfield, "Improved watershed transform for medical image segmentation using prior information," *IEEE Transactions on Medical Imaging*, vol. 23, pp. 447–458, Apr. 2004.

[66] F. Meyer and S. Beucher, "Morphological segmentation," *Journal of Visual Communication and Image Representation*, vol. 1, pp. 21–46, Sept. 1990.

www.manaraa.com

Chapter 2

Segmentation, Feature Extraction & Clinical Applications

2.1 Introduction

The purpose of applying image processing techniques to the histopathology ranges from cell counting and cell type classification, to calculating quantitative measurements of morphological, histochemical and immunohistochemical features from images, and determining whether a specific pathology is present within the tissue samples. Numerous commercial pathology analysis platforms are available with the increase of whole slide imaging systems in digital pathology, thus improvements have been made in both the quantity and quality of data collected from histological analysis [1].

Despite the International League Against Epilepsy (ILAE) classification system for focal cortical dysplasia (FCD), there is still a lack of research towards automated and quantitative methods that are able to accurately characterize dysplastic lesions in epilepsy. Field fraction estimate is a commonly used measure, utilized in histology analysis and represents the fraction of positively stained pixels in each field [2]. However, with respect to cortical architecture, field fraction is less sensitive to the reciprocal nature of size and

www.manaraa.com

density within cortical layers. The addition of more specific and sensitive measures in localized regions will allow for better analysis and detection of architectural abnormalities.

Another study assessed measurements of cellular profiles (cell body area/size), cortical thickness, myelination and number of heterotopic neurons in white matter and performed a correlation study with the patients ILAE guided FCD [3]. Although this methodology presented a semi-quantitative approach in assessing morphological parameters for FCD subgroups, further work is required to better quantitatively characterize whole sections of cortical tissue, including an automated approach.

Neuron density is often studied in white matter regions [4] since increased neuron populations in white matter is indicative of FCD [5], however, more detailed and informative measures such as neuron size, neuron density, neuron clustering, neuron orientation, and neuron eccentricity are needed to better quantify and assess the full cortical architecture in epilepsy. Typically, neurons are radially oriented within the cortex, however in many disease states including epilepsy, mal-orientation occurs during the radial migration process of development [6]. In the same way, abnormal neuron migration during cortical development may cause clustering in particular regions of the cortex. Additionally, neuron eccentricity has also been shown to present as abnormal in disease states, as it is indicative of neuron morphology and is therefore a beneficial feature is assessing neuronal abnormalities [7,8]. Overall, there is a need for a more automated method that can apply the ILAE classification of FCD, resulting in better detection of abnormalities in the cortex. The work in this thesis focuses on features present in FCD categories Type I and II.

In this chapter I present a technique to automatically segment neurons from Immuno-HistoChemistry (IHC) stained histology slides and extract relevant features, to assess the architecture and abnormalities of neuronal tissue. The proposed method uses colour deconvolution, histogram thresholding and marker-based watershed segmentation to delineate individual neurons before extracting relevant neuronal features. This study also

www.manaraa.com

presents the clinical applications and relevance of using more specific neuronal measures in assessing FCDs in temporal lobe epilepsy (TLE).

2.2 Methods

2.2.1 Patient Recruitment and Surgery

Patients suffering from medically intractable TLE and candidates for anterior temporal lobectomy (ATL) were recruited as part of a ongoing research study at the Robarts Research Institute. Of this cohort, a subset of twelve patients were selected for analysis within this project. This subset included patients with available NEUN stained neocortex slides since other patients had only mesial structures and alternatively stained slides available. Patients were also divided into two groups for clinical analysis, those with verified FCD in the pathology report and those without documented FCD. The non-FCD patients had no report of architectural abnormalities.

This study was approved by the Health Sciences Research Ethics Board of Western University, and informed consent was received from all patients before participation. Patients were scanned pre-operatively in clinical 1.5T Magnetic Resonance Imaging (MRI) and were assessed with scalp electroencephalograghy (EEG) for seizure characterization. In addition to the clinical protocols, patients were also scanned in 3T and 7T MRI research scanners at Robarts Research Institute. Table 2.1 summarizes the relevant patient data used in this study.

2.2.2 Histological Processing

Following surgery both the hippocampus and neocortex were retrieved from the operating room and fixed in a 10% formalin solution overnight. The specimens were then scanned in a 9.4T MRI at Robarts Research Institute. while immersed in a silicone-based lubricant(Fomblin PFPE Lubricant, Solvay) to reduce air-tissue surface artifacts. The

www.manaraa.com

Subj ID	Sex	Age	Seizure Origin	Pathology	MRI	Validation
EPI_P006	F	22	R	gliosis	normal	Y
EPI_P008	F	40	L	gliosis	incidental	Y
EPI_P015	F	40	R	gliosis, mild CD	abnormal	Y
EPI_P016	F	25	L	gliosis, atypical cells in WM	incidental	Y
EPI_P021	M	20	L	gliosis, minor architectural abnormalities	abnormal	Y
EPI_P027	F	41	R	gliosis	abnormal	
EPI_P033	F	32	L	gliosis	abnormal	Y
EPI_P036	M	39	R	FCD type 1b, gliosis	abnormal	Y
EPI_P037	M	23	L	gliosis, multifocal lesions, FCD type 1a	normal	
EPI_P040	M	34	L	gliosis, focal minor neocortical abnormalities	abnormal	Y
EPI_P043	F	33	R	gliosis	abnormal	
EPI_P044	M	39	R	gliosis, FCD type Ic	abnormal	Y

Table 2.1: Summary of patient demographics and clinical information including gender,age, seizure origin, histopathological findings in neocortex and MRI findings. Patients used in the segmentation validation are denoted in the last column with 'Y'. Clinical MRI findings may also indicate abnormal findings in the hippocampus

specimens underwent a standard histological processing protocol of fixation, embedding, sectioning, staining and digitization, performed at the Department of Pathology at London Health Sciences Centre - University Hospital. During this process the tissue specimen was cut through the coronal plane into two halves, anterior and posterior. Each half of

www.manaraa.com

the specimen was then embedded in agar for stabilization during the slicing process. The specimens were sectioned into 4.4 mm pieces in the anterior to posterior direction and parallel to the initial cut, using a standard deli slicer. Each block was embedded in paraffin for sectioning and placed on a microtome where 8 µm sections were cut from the face of each block and mounted onto slides for staining.

For both hippocampal and neocortical specimens, one slide from each block was stained with hematoxylin and eosin (H&E). Glial fibrillary acidic protein (GFAP) (polyclonal antibody) and neuronal nuclei (NeuN) (monoclonal antibody) were used for every other block. Additional stains were ordered when necessary for diagnosis by the pathologist. Following staining, the resulting histology slides were digitized on a ScanScope GL (Aperio Technologies, Vista, CA, USA) bright field slide scanning system in BigTIFF file format, using a pixel resolution of 0.5 µm. Figure 2.1 shows an overview of the histology processing steps described.

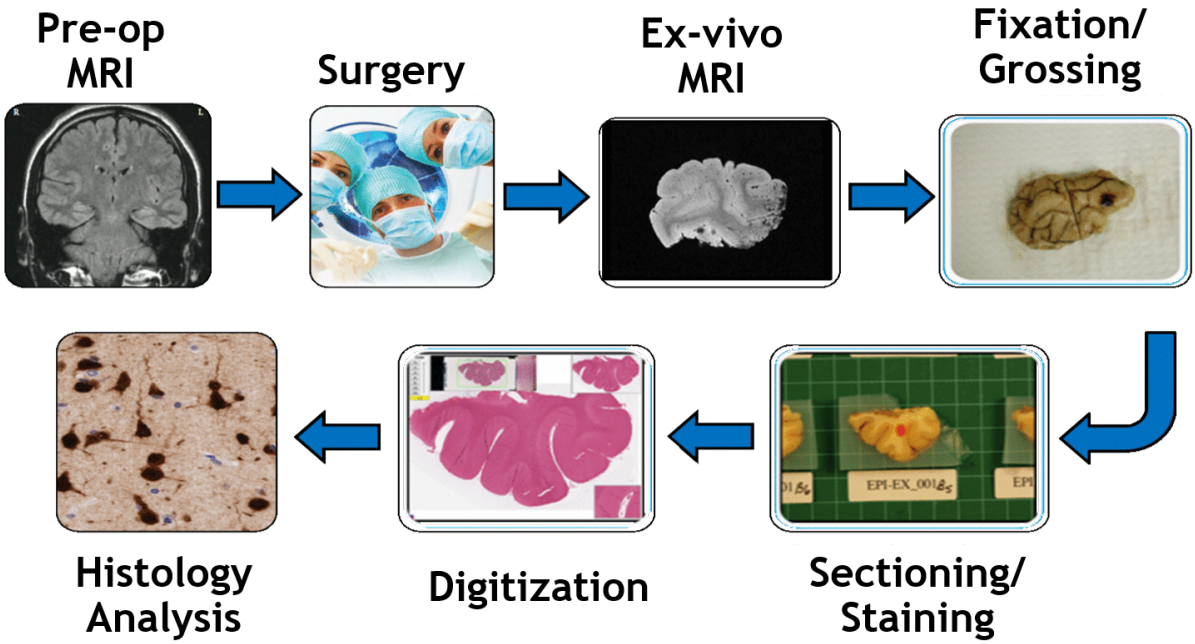

Figure 2.1: Pipeline outlining histological processing

www.manaraa.com

Several factors create limitations that dictate the protocols in tissue processing. The committee governing tissue for research purposes requires that the remaining part of the specimen blocks be reserved in a tissue archive in the case any future analysis is needed. In addition the number of subjects in our study and number of stained sections available is restricted due to the significantly increased costs associated with acquiring and processing serial sections for both hippocampal and neocortical tissue specimens.

2.2.3 Programming Language

All programs for this project were written using MATLAB (The MathWorks Inc) version 9.0.0.341360 (R2016A), Service Pack 1, along with the Image Processsing Toolbox.

2.2.4 Neuron Cell Body Segmentation

The main challenges in segmenting cells in histology specimens, result from the fact that the specimen is a 2-D representation of a 3-D tissue sample. This sectioning can result in partially imaged nuclei, imaging of cells at non-conventional angles and damage due to the sectioning process [9]. Furthermore, specimen sections have a finite thickness resulting in overlapping or partially superposed cells and nuclei, often making it difficult to determine one cell from its neighbour. Finally, imaging noise in the background regions and other image artifacts result in additional errors. The end result of these limitations is a set of objects that may differ considerably from the ideal cell shape *in-vivo*. The goal of this study is to develop an efficient and accurate algorithm for detecting and segmenting cells in 2-D histological images. This is a necessary step towards quantifying aspects of both normal and diseased tissue architecture, therefore it is important to detect the correct number of cells with high accuracy, and to delineate them with minimal human effort.

This detection method involves a two-step process in which the images first undergo a colour deconvolution algorithm [10,11] to separate individual colour staining within the slide, followed by a marker-based watershed segmentation [12]. The overall segmentation

www.manaraa.com

process is illustrated in Figure 2.2.

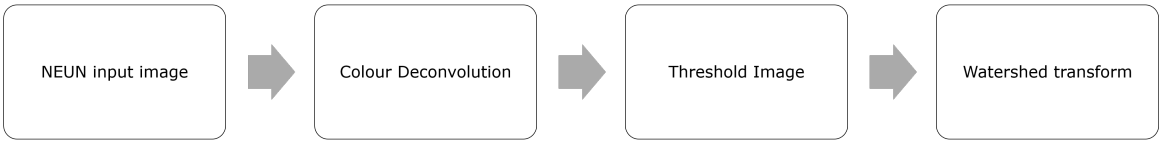

Figure 2.2: Flowchart outlining the main steps of the proposed neuron segmentation algorithm

Colour Deconvolution

In image processing, colour deconvolution is used to separate an image into three individual colour channels, indicating the distribution of stains used. This allows for the detection of proteins and also allows for the digital segmentation of various cellular structures within a tissue sample. In the case of this research, the slides were stained with both Haematoxylin and diaminobenzidine (DAB) chromogens, which appear as blue and brown, respectively. The primary stain colour of interest is brown due to the DAB chromogen applied with NeuN antibody to stain the neuronal cell types in the histology slides. The colour deconvolution method [10] is based on the orthonormal transformation of an RGB image to a single colour channel and stain specific values for the optical density can be determined by the relative absorption for red, green and blue on signal stained slides. The normalized OD matrix for haematoxylin and DAB can be seen in Table 2.2 [11]. This method allows for the determination of stain densities in multiple stained slides, providing a separation of the Haematoxylin and DAB staining. The process of translating the initial NEUN image to the deconvolved stained image can be seen in Figure 2.3.

www.manaraa.com

Stain Type	R(red)	G(green)	B(blue)
Haem	0.650	0.704	0.286
DAB	0.268	0.570	0.776

Table 2.2: The normalized OD matrix for haematoxylin and DAB

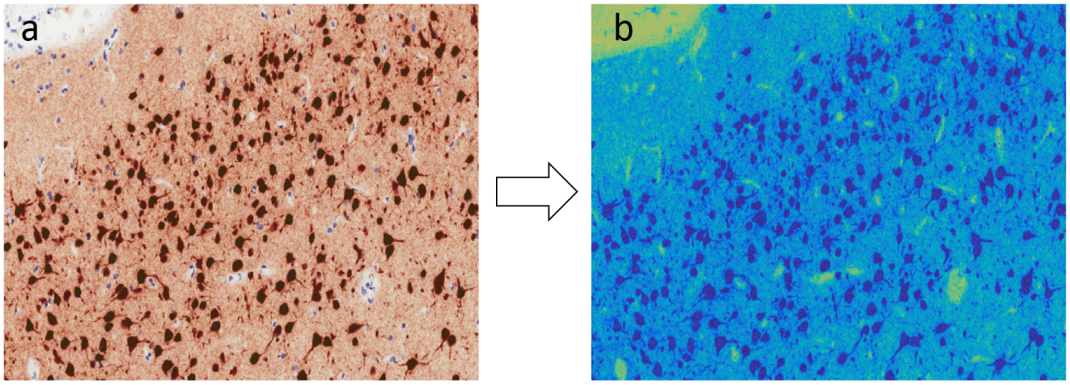

Figure 2.3: An example of colour deconvolution. This section is taken from a smaller sampled image to show the neurons that will be segmented. a) Original NEUN image b)Stain specific colour deconvolution algorithm applied to image, dark blue refers to the positive DAB colour indicative of a neuronal cell type

Marker-Based Watershed Segmentation

A marker-based watershed algorithm was selected to segment neurons within each slide. In general, a watershed transformation provides a means to separate overlapping objects and also allows for a lower computation time and better accuracy compared to other existing methods [13]. Specifically, a marker based watershed algorithm decreases the over-segmentation problem of watershed algorithms by reducing the number of minima within an image [14, 15]. The basic outline of the segmentation process used in this research is shown in Figure 2.4.

This algorithm is based on the fact that an image can be considered as a topographic

www.manaraa.com

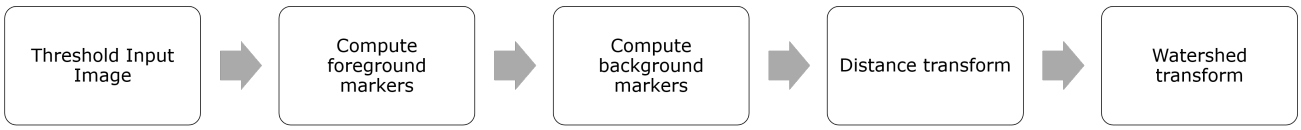

Figure 2.4: Flowchart outlining the steps of the watershed segmentation

surface where the gradient image gray-levels represent varying altitudes, as seen in Figure 2.5. Edges correspond to high watersheds while low-gradient object interior correspond to catchment basins. These catchment basins are homogeneous regions in which all pixels are connected with the basin's minimum altitude (gray-level). The basins then represent the regions within the resulting segmented image. Typically, watershed segmentation algorithms may produce highly over-segmented images with hundreds of catchment basins, therefore, in order to overcome this problem region markers can be applied to generate better segmentation results.

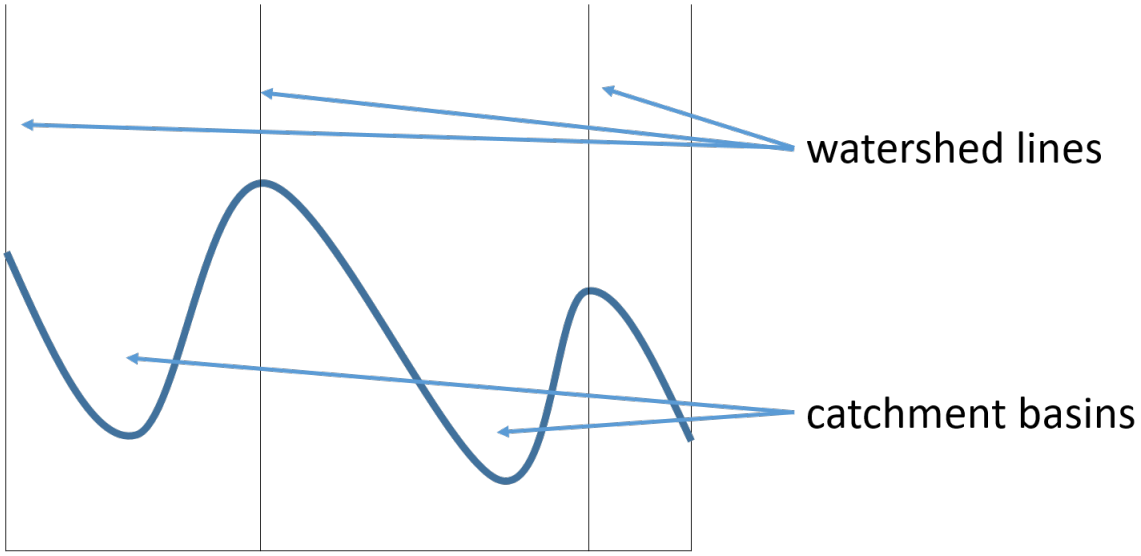

Figure 2.5: One-dimensional representation of watershed segmentation with a gray level profile of image data. Local minima yield catchment basins and local maxima define the watershed lines

www.manaraa.com

The first step in the segmentation process is to clean up the image, allowing for easier processing in selecting foreground and background markers. This involves the use of morphological operations of opening by reconstruction (an erosion followed by reconstruction), to smooth the outside of the neurons and closing by reconstruction (dilation followed by reconstruction) in order to smooth the inside of the neurons. This combination of morphological operations allows for the creation of flat maxima inside each neuron.

The complement of the reconstructed image is computed where in a binary image, zeros become ones and ones become zeros. From this complement, the regional maxima within the image can be determined. This creates a mapping of neuron centres within the image, also known as the foreground markers to indicate areas of the image to be included in the segmentation. The foreground markers are further processed to remove small amounts of neuron debris and markers too small to be considered as a neuron. The threshold for this is calculated such that the minimum area of a granule cell is approximately 15 μm^2, following erosion in MATLAB with a 5x5 kernel. Anything smaller than this is removed from the image.

The background of the image is marked using a thresholding operation, followed by the computation of a skeleton by influence zones to thin the background such that pixels in the background markers do not touch those in the foreground neuron markers. These influence zones are computed using the watershed transform of the distance transform of the thresholded image, and from this the watershed ridge lines can be determined. The final step in the process is to compute the watershed transform of the segmentation function. A gradient magnitude was used as the segmentation function since the gradient is high at the borders of the objects but low within the objects. The gradient magnitude image is also modified so that the regional minima occurs only at foreground and background marker pixels and from this the watershed segmentation can be computed. Images generated demonstrating this process can be seen in Figure 2.6. The resulting

www.manaraa.com

segmentation can be used to extract neuron borders within the image, allowing for a fully segmented binary image of neuron locations.

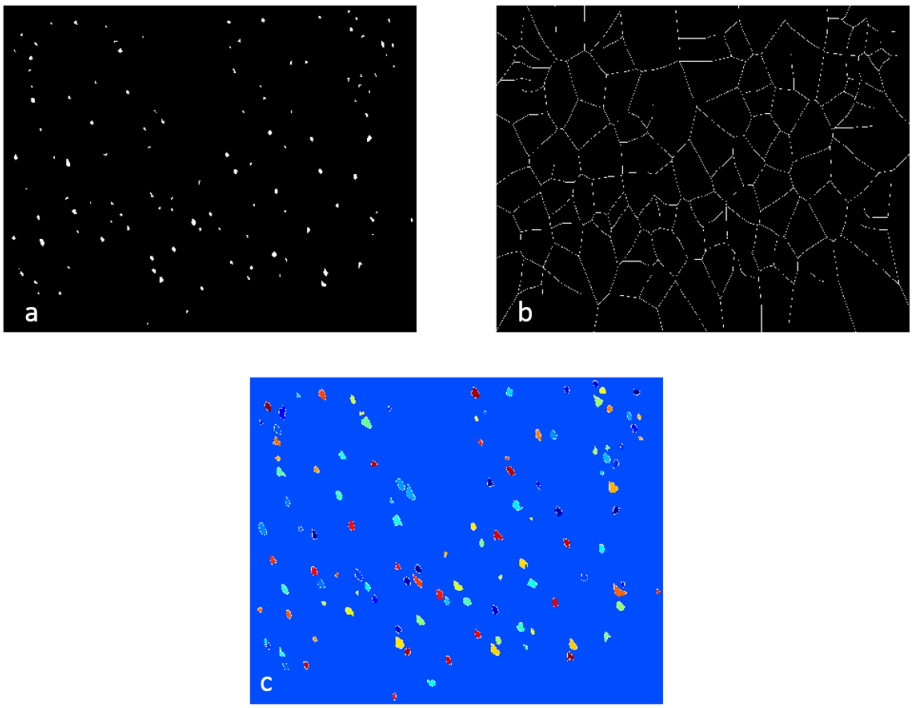

Figure 2.6: a)Flat maxima 'markers' indicating neuron positions b)watershed ridge lines, based on the distance transform c) coloured watershed label matrix

2.2.5 Feature Extraction

Following segmentation, each slide was systematically divided into square tiles of size 100 µm x 100 µm, i.e. 200 x 200 pixel. For each tile, histopathologic features were extracted and maps of each feature were later generated for every histology slide. The features used included neuron count (density), neuron size (area), orientation, clustering, eccentricity and field fraction, detailed as follows.

neuron density is evaluated as the number of neurons per unit volume and was extracted from an automated count of each neuron within a tile. Clinically, density

www.manaraa.com

may be an indicator of FCD in areas where there is significantly decreased neuron density.

neuron size is calculated by the total number of pixels within a single neuron (from MATLAB regionprops metric, area) and can be represented as area in μm^2. Most often in epilepsy, large neuron size can be indicative of balloon cells, present in Type IIb FCD.

orientation is a scalar value that specifies the angle in degrees between the x-axis and major axis of the neuron's inertia ellipse that has the same second-moments as the region. The MATLAB function, region property (regionprops), orientation, was used for this feature measurement. Since neuron orientation relies on other factors, such as slide orientation during digitization, this measure was calculated as a variance of angle rather than the exact value for clinical analysis. Orientation is indicative of malformations in cortical development and is included in FCD Type IIa [16].

clustering is calculated based on the mean Euclidean distance matrix of a set of neurons and uses the MATLAB centroid to perform a pairwise distance calculation between all neurons in the specified field. An adjaceny matrix is used to compare each neuron to its neighbours. Clustering is also present in disease states as a result of malformations in cortical development.

eccentricity is a measure of deviation from circularity in an object. This is measured using MATLAB regionprops, eccentricity, and is the ratio of the distance between the foci of the ellipse and its major axis length. The value is represented a scalar between 0 and 1 for each neuron. As mentioned previously, eccentricity is indicative of neuron morphology and therefore may be capable of assessing FCD in epilepsy.

field fraction estimate is a commonly used measure representing the fraction of posi-

www.manaraa.com

tively stained pixels in each field. Since field fraction is sensitive to the density and size of cortical layers, the field fraction estimate is used to highlight the importance of using other measures to analyze the cortical architecture.

2.2.6 Validation

To evaluate the performance of a segmentation technique the aim is to compare newly developed and existing methods. In these sections, I will introduce metrics to quantitatively compare methods within an experimental trial and consider caveats of employing them for different segmentation problems.

A gold standard method can be considered a benchmark to test against, however actual ground truth knowledge is often not available. It has been established in medical imaging that a surrogate gold standard is an expert interpretation of an image in the form of a manual annotation, commonly found in the image segmentation literature as label maps resulting from manual segmentations. In literature, the accuracy of a segmentation method is determined in its score against a gold standard benchmark in terms of a specific metric. Such a validation metric allows the accuracy of a segmentation to be quantified. In this study the Dice similarity coefficient [17], a regional based metric, was used in order to assess segmentation accuracy. The Bland-Altman difference plot was also used to compare inter-rater reliability in addition to the performance between manual and automated segmentation techniques.

Manual Segmentation

The same slide set that was employed for automated analysis was used for the manual segmentation. In order to validate the accuracy of the segmentation, manual neurons counts were performed systematically and compared to the resulting automated segmentation metrics. A protocol (see Appendix A) for manual neuron counting was established with the following restrictions: Regions of Interest (ROI) were selected from the cortex in

www.manaraa.com

Aperio ImageScope software in field of size 500 µm x 250 µm. The ImageScope positive pixel count algorithm was applied to the ROI in order to indicate the NeuN staining within the image. Neuron size was measured to have at least a diameter of 4 µm [18], using the ImageScope ruler tool, and general neuron appearance was evaluated, according to the prescribed protocol. Neurons touching the edge of the field of view were not included in the total count to ensure only whole neurons where assessed. This was also accounted for within the automated algorithm to maintain consistency. Neurons were manually contoured in ITK-Snap software [19] and imported into MATLAB for further analysis and comparisons.

Dice Similarity Coefficient

We used the Dice similarity coefficient as a measure of spatial overlap accuracy in the evaluation of performance in automated and manual segmentation. It was also used in this research as a validation metric of reproducibility between manual raters.

$$DSC = \frac{2(A \cap B)}{A + B} \tag{2.1}$$

where A defines the manually segmented region and B is the region obtained from the segmentation algorithm output. This is illustrated visually in Figure 2.7. In segmentation validation literature, Zijdenbos *et al.* [20], defined image segmentation as having a good overlap when DSC > 0.7.

www.manaraa.com

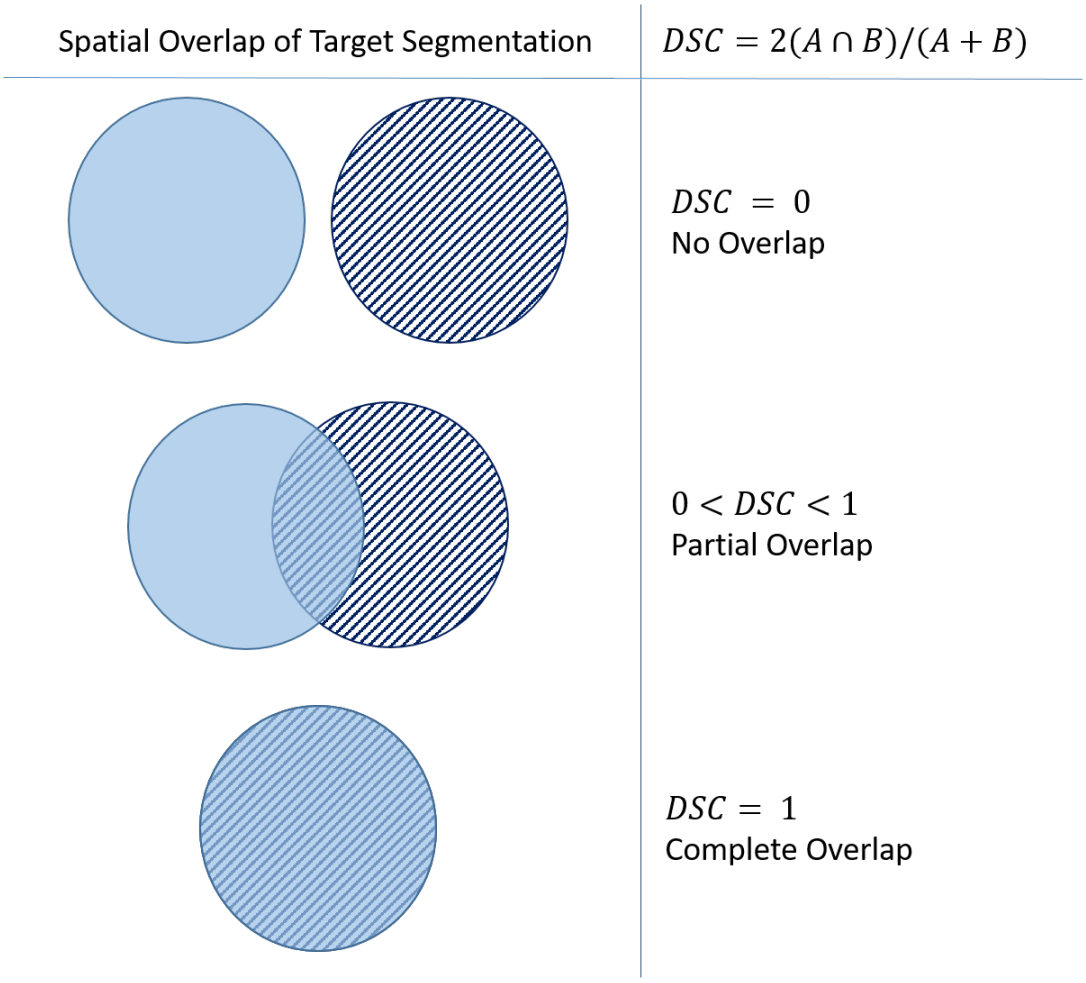

Figure 2.7: Dice similarity coefficient as a measure of segmentation validation

www.manaraa.com

Bland-Altman Difference Plot

The Bland-Altman plot [21], or difference plot, is a graphical method to compare two measurements techniques. This method is used to calculate the mean difference between two quantitative measurements and constructs the limits of agreement, reporting the 95% limits. An example plot is shown in Figure 2.8. Bland-Altman plots offer another approach to assessing agreement between measures, particular when two observers or raters are assessing the same variable. Bland-Altman analyses provide information about the interchangeability of two measures without assuming that either is the gold-standard and can be of value in clinical settings. Additionally, Bland-Altman can be used to compare a new technique with a gold standard, which in this case we compare the automated segmentation with the assumed gold standard - the manual segmentation.

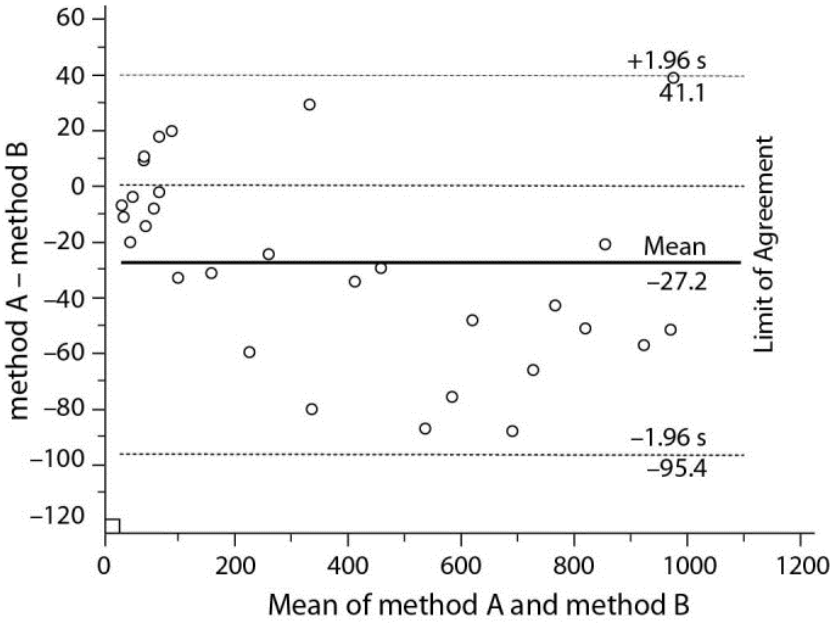

Figure 2.8: Example Bland-Altman Plot shows the difference between two methods. Mean difference is -27.2 while the limits of agreement extend from -95.5 to 41.1. Plotting the difference against mean also allows for investigation of the relationship between the measurement error and the ground truth value. The visual examination of the plot also allows for the evaluation of global agreement between the two measurements

www.manaraa.com

Orientation Feature Validation

A secondary validation was performed in order to assess the quality of the automated neuron orientation analysis and a similar protocol to the contouring segmentation was followed (see Appendix B). The orientation annotations were performed on previous segmentations and only one raters slides were used. A straight line was drawn through the centre of the neuron, with the orientation following the cell body from base to apex of the neuron. The resulting annotations were imported into the MATLAB software for analysis and comparison with the automated feature map of the same slide. To accurately compare the distance between two given angles, a correction was applied to one set of angles such that only the shortest distance between two angles was considered. This correction does not change the data or orientation of the neuron but simply allows for a more accurate representation of the distance between two neurons. A visual representation of this angle correction can be seen in Figure 2.9

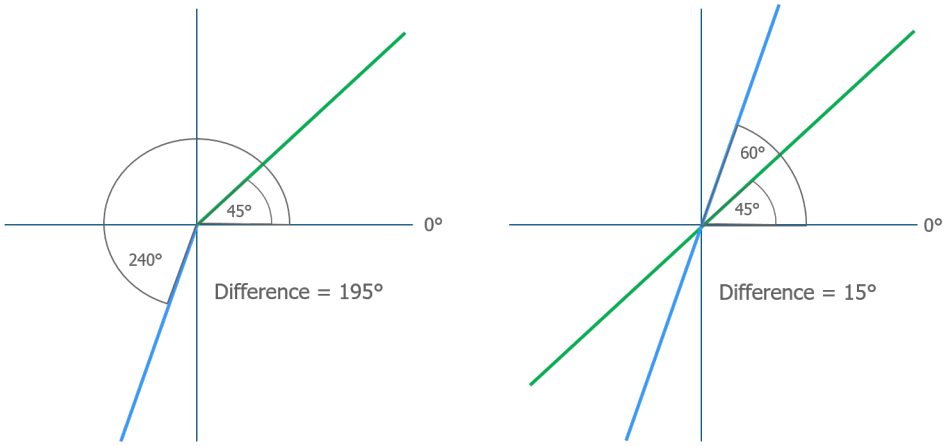

Figure 2.9: Angle correction applied such that only the smallest angle difference is considered

Spearman's Rank Correlation Coefficient

Correlation is a statistical technique that can shows if pairs of variables are linearly related and how strong this relationship is in a value between -1 and 1. The stronger

www.manaraa.com

the correlation, the closer the correlation coefficient approaches 1 or -1. A correlation coefficient of zero indicates that a relationship does not exist between the two variables [22].

Specifically, Spearman's Rank correlation coefficient [23] is a technique which can be used to assess the strength and negative or positive direction of a relationship between two variables. It is considered to be useful when one or both variables are skewed and is robust when there are extreme values [22].

2.2.7 Clinical Analysis

In order to assess the relevance of the described algorithms and features in terms of a clinical setting, for each patient slide, manual labels were created in Aperio Image Scope (Leica Biosystems) to delineate the 6 individual layers, seen in Figure 2.10. The protocol for the manual layer segmentation is described in Appendix C. Only areas in which the slide could be considered non-tangential cuts were included. In addition, any areas with staining or other artifacts were excluded from the analysis.

These labels were imported into MATLAB and used as masks for the feature map data. The patient data was divided into two categories for comparison, those patients with pathologist verified cases of FCD (sample size = 3) and those without (sample size = 6). These masks were used to investigate whether layer-specific estimates of the selected features are different between cortex without any identified pathology and those with FCD. Cortical lamina was chosen to summarize each feature, since these features can vary greatly across lamina and add additional variability to this comparison.

Two-way ANOVA

A two-way repeated measures anaylysis of variance (ANOVA) was used to determine differences between the two patient groups and also between the six cortical layers for each feature type (size, density, orientation, eccentricity and field fraction), These tests

www.manaraa.com

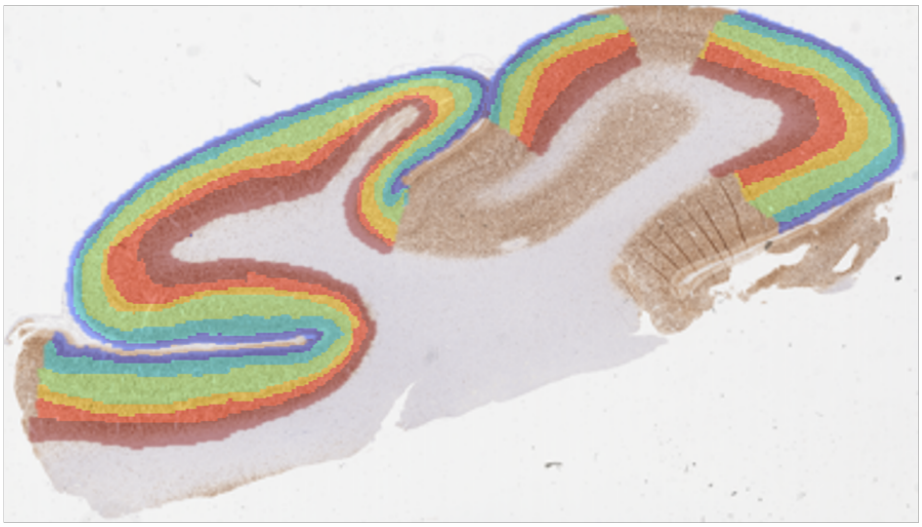

Figure 2.10: Layer label for EPI_P037. Each colour represents a manually annotated layer, from the pial in dark blue (layer 1) to layer 6 in dark red.

were corrected using Holm-Bonferroni multiple-comparison correction method and the alpha (p) value was set to 0.05.

Holm Bonferroni Correction

When several hypotheses are considered, the problem of multiplicity becomes apparent: The more hypotheses that are checked, the higher the probability of false positives occurring. The Holm-Bonferroni [24] method is an approach used to control the false-positive error rate. All p-values are sorted in order of smallest (most significant) to the largest. If the 1st p-value is greater than or equal to alpha/n, where n is the number p-values, the procedure is stopped and no p-values are considered to be significant. Otherwise, the 1st p-value is significant and now the second p-value is compared to alpha/(n-1). This process continues until the p-values are no longer significant or the correction has been applied to all p-values.

www.manaraa.com

2.3 Results

2.3.1 Examples of Neuron Segmentation & Feature Maps

Figure 2.11 shows a visual depiction of the resulting segmentation. Our approach corrects for under-segmentation and allows visually joint neurons to be separated. The complete method gives a good final segmentation and the statistical results are presented in the validation sections below.

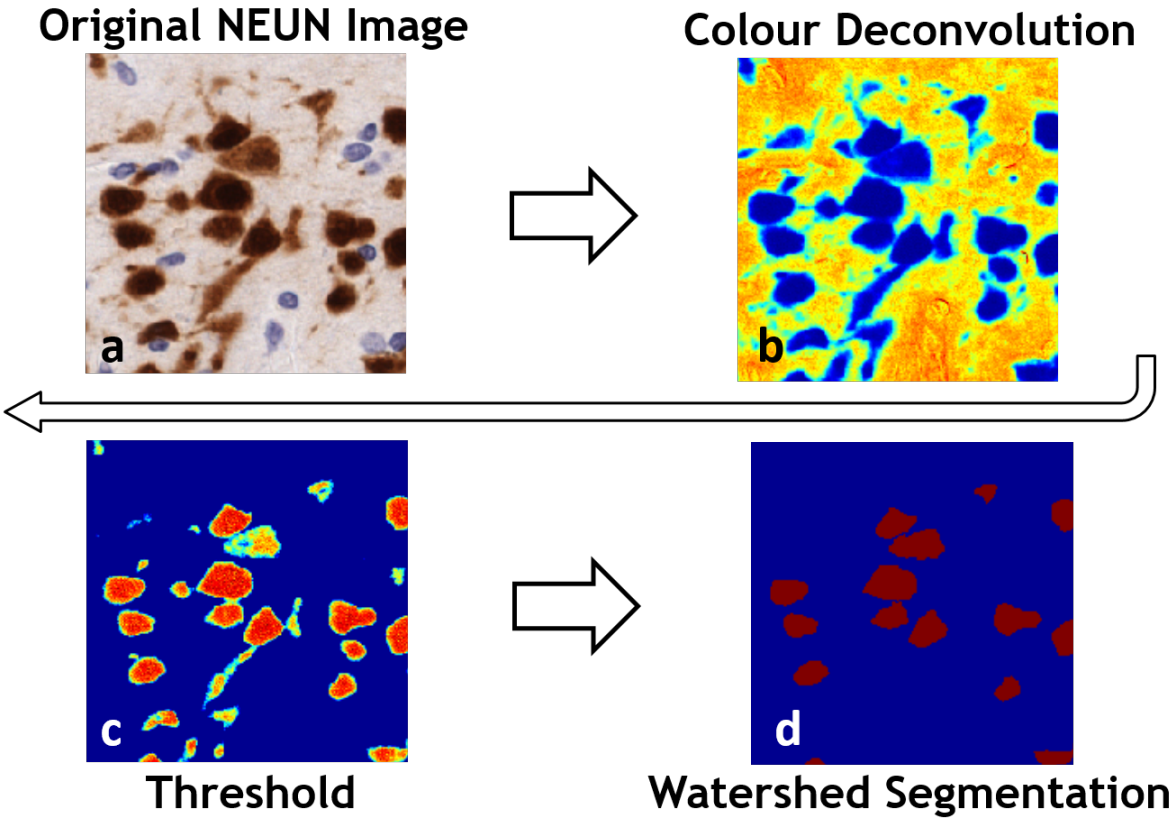

Figure 2.11: Example of (a) original NEUN image, (b) colour deconvolution (c) image thresholding and (d) watershed segmentation

The resulting segmentation allowed each of the features to be applied to individual neurons and measurements taken. The following images are the whole-slide feature maps

www.manaraa.com

generated from the application of the segmentation described previously in Section 2.2.4, followed by various neuron feature measurements applied to NEUN histology slides. Images in Figures 2.12 and 2.13 were generated using MATLAB.

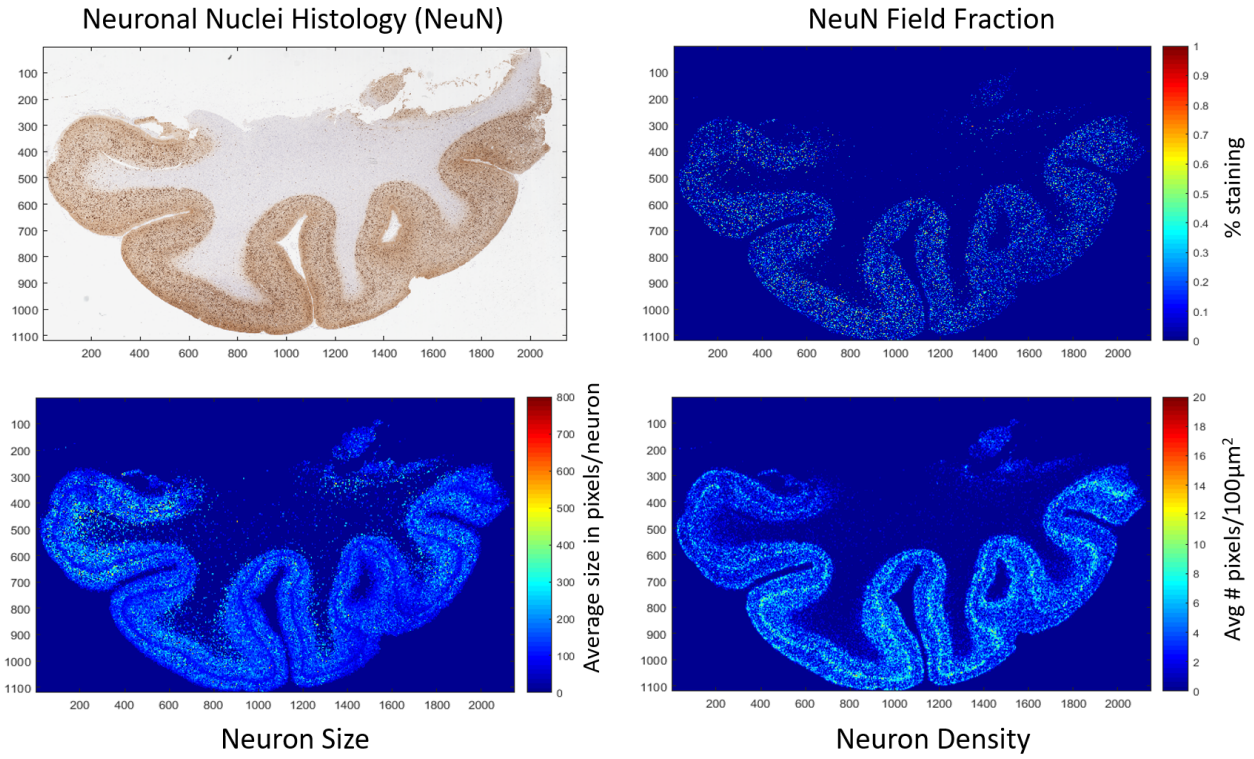

Figure 2.12: Example of feature maps generated for Field Fraction, Neuron Density and Neuron Size. The feature maps are generated from averaged values within a 100 µm^2 section.

www.manaraa.com

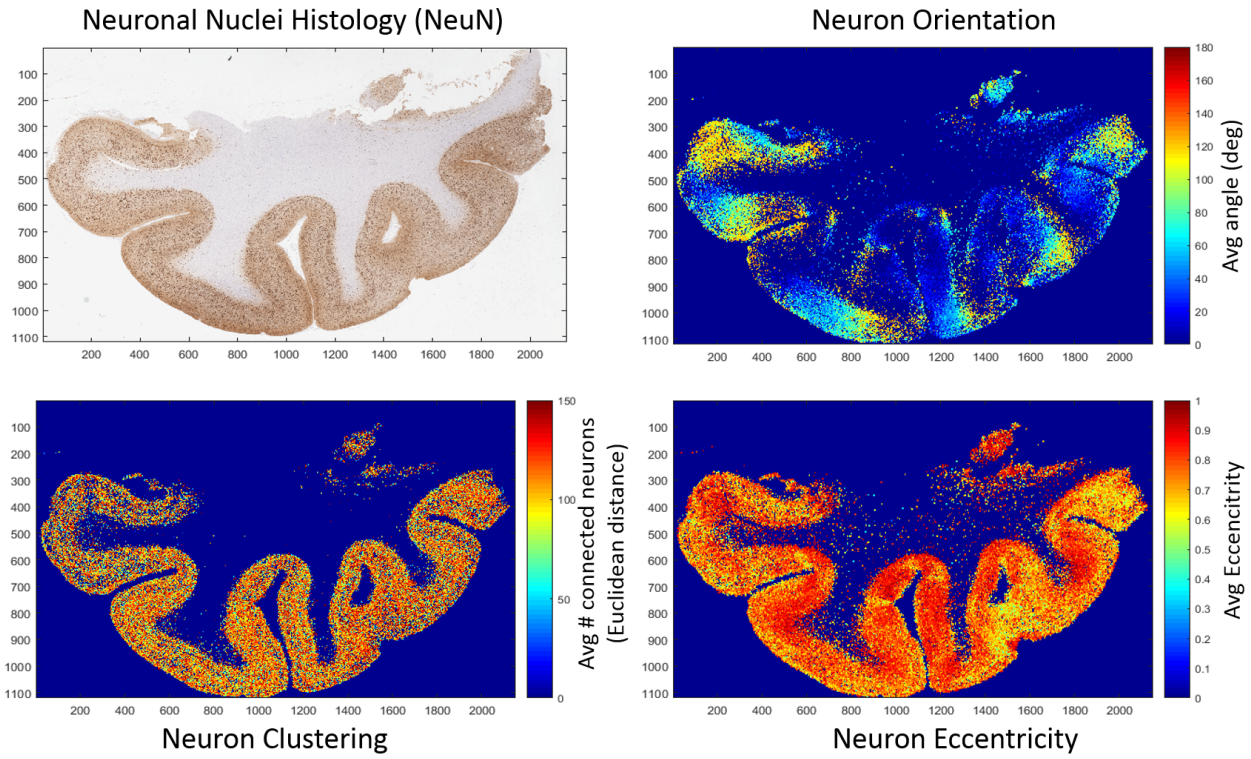

Figure 2.13: Example of feature maps generated for Orientation, Clustering and Eccentricity. The feature maps are generated from averaged values within a 100 µm section.

www.manaraa.com

Inter-rater correlations

The Dice similarity coefficient (DSC) was also used to validate and evaluate the spatial overlap between manual segmentations and reproducibility in neuron histology images, illustrated on nine clinical examples. Table 2.5 displays the Dice similarity coefficient of each subject comparing the overlap of segmentations from two different raters. The mean DSC of 0.87 (range [0.86, 0.88]) was within the range of good reproducibility, as defined by Zijdenbos *et al* in literature regarding image segmentation, where a good overlap is regarded to have DSC > 0.70 [20].

Subj ID	Dice
EPI_P006	0.88
EPI_P008	0.86
EPI_P015	0.87
EPI_P016	0.86
EPI_P021	0.88
EPI_P033	0.87
EPI_P036	0.86
EPI_P040	0.88
EPI_P044	0.86

Table 2.3: Dice Similarity Coefficients for inter-rater reliability in manual segmentations

The intraclass correlation coefficient for absolute agreement of average number of neurons in a FOV was 0.97 (95% CI +0.89 to +0.99) while the ICC for average size of neurons was 0.95 (95% CI +0.81 to +0.99).

The following Bland-Altman plots, in Figures 2.14 and 2.15, compare both size and density between the two raters. The Bland-Altman plot for density demonstrates similar results to that of the automated and manual comparison. The mean discrepancy is low and the limits of agreement are acceptable to the clinical application of this method.

www.manaraa.com

There is no observable trend towards the amount of neurons within a given region.

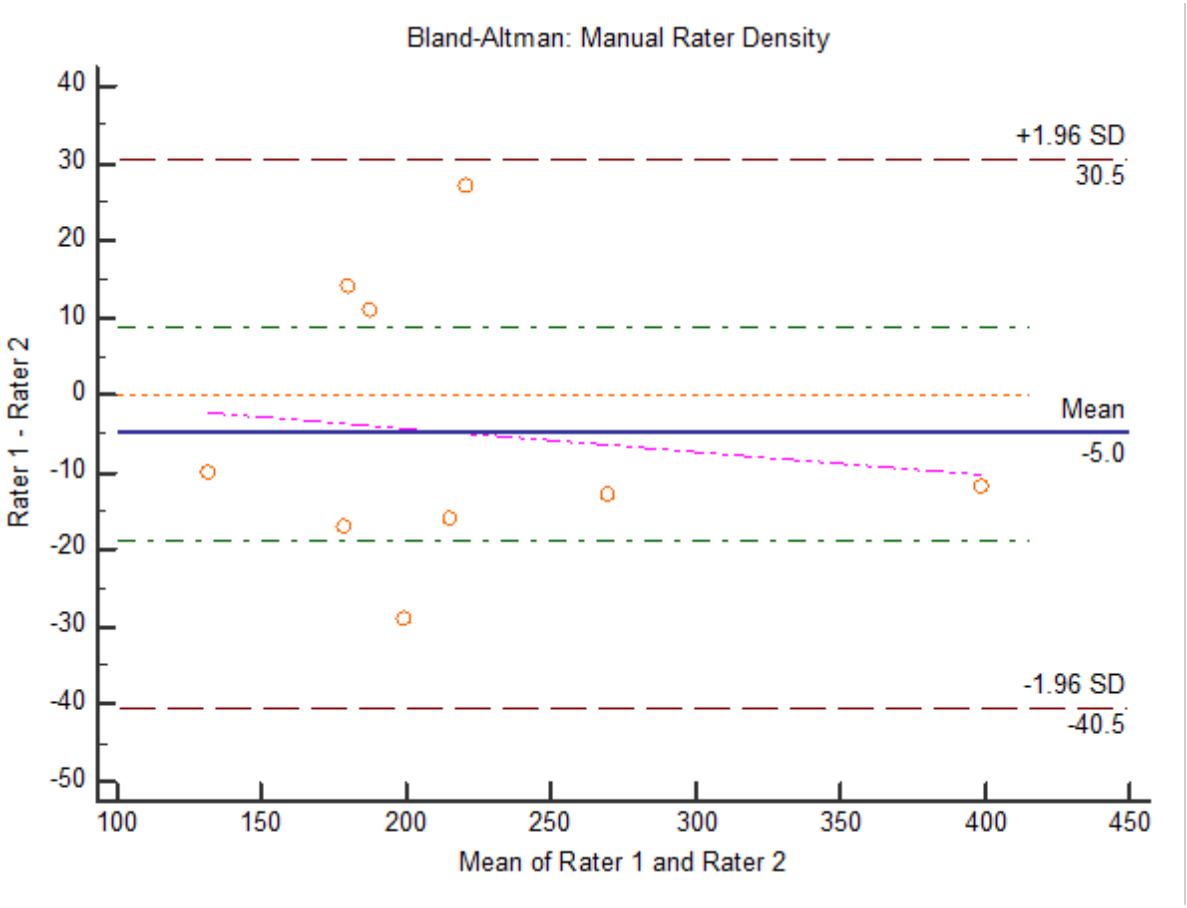

Figure 2.14: Bland Altman plot comparing mean neuron density measurements across two raters

The Bland-Altman plot for size has a very low mean discrepancy, indicating that the two raters more similarly follow the neuron boundary in annotations, compared to the previous resulting plot between manual and automated methods. The limits of agreement are somewhat wide, but considering the inherent variability within neuron size, these values can be considered acceptable.

www.manaraa.com

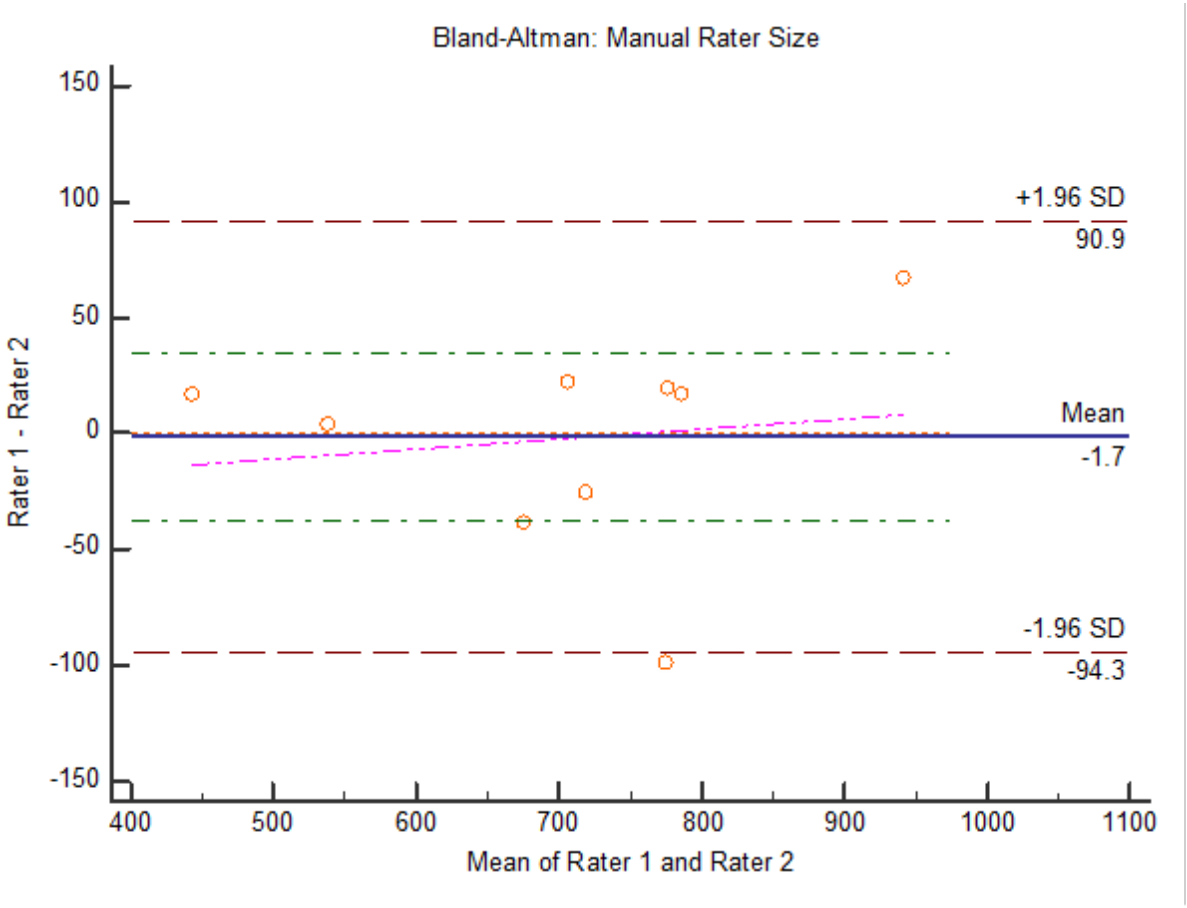

Figure 2.15: Bland Altman plot comparing mean neuron size measurements across two raters

www.manaraa.com

2.3.2 Automated Contouring Validation

The Dice similarity coefficient (DSC) was used as a statistical validation metric to evaluate spatial overlap and the performance of manual segmentation reproducibility in neuron histology images, illustrated on nine clinical examples. Table 2.5 displays the Dice similarity coefficient of each subject comparing the overlap of segmentations from two different raters. The mean DSC of 0.77 (range [0.60,0.81]) was within the range of good reproducibility (as defined by Zijdenbos) [20]. The Zijdenbos method of similarity has been utilized previously in histological studies, verifying its ability to measure consistent overlap in cell segmentation [25, 26].

Subj ID	Dice
EPI_P006	0.60
EPI_P008	0.80
EPI_P015	0.81
EPI_P016	0.73
EPI_P021	0.80
EPI_P033	0.80
EPI_P036	0.79
EPI_P040	0.79
EPI_P044	0.80

Table 2.4: Dice Similarity Coefficients for comparing overlap between automated and manual segmentations

The intraclass correlation coefficient (ICC) for absolute agreement of average number of neurons in a region of interest was 0.96 (95% CI +0.86 to +0.99) while the ICC for average size of neurons was 0.38 (95% CI -0.20 to +0.82). Although seemingly low, the ICC for size represents an under-segmentation in the automated algorithm, resulting from morphological operations such as erosion and dilation. As demonstrated in the DSC

www.manaraa.com

values, in the majority of cases, the neuron placement is correctly located.

The following Bland-Altman plots, in Figures 2.16 and 2.17, compare both size and density between the manual segmentation and the automated segmentation. For density, the average discrepancy is 6.1 neurons. Clinically, we can assume that this is a reasonable degree of variability between automated and manual slides considering that most of the regions used contained several hundred neurons. The limits of agreement, although somewhat wide are still within reasonable quantities relevant to the application. There is no observable trend in the data as indicated by the regression line.

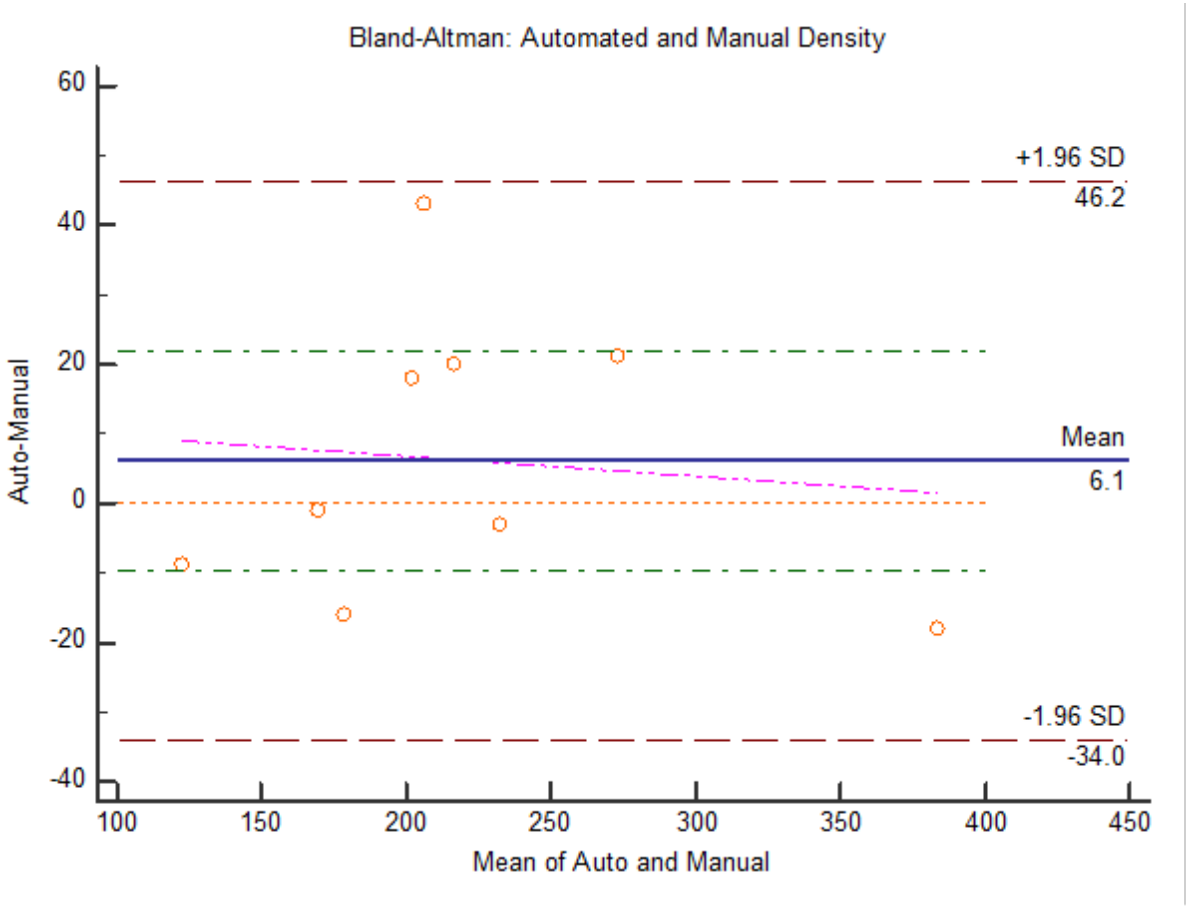

Figure 2.16: Bland Altman plot comparing mean neuron density measurements between the automated and manual segmentations

Comparatively, the Bland-Altman Plot in Figure 2.17 compares the size metric of the

www.manaraa.com

automated and manual techniques. There is a significantly under-estimation of size in the automated method and this difference increases with larger neuron size. The limits of agreement are also very wide.

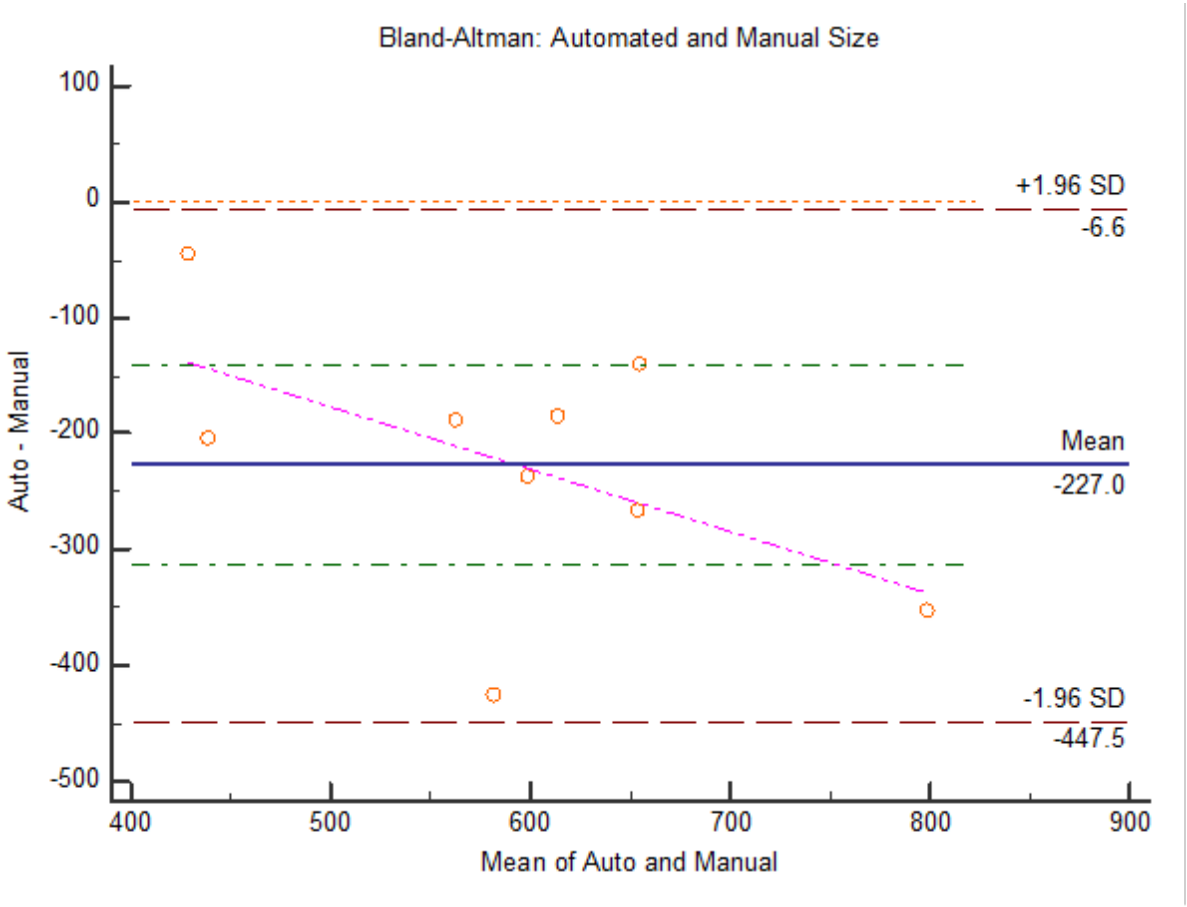

Figure 2.17: Bland Altman plot comparing mean neuron size measurements between the automated and manual segmentations

www.manaraa.com

2.3.3 Orientation Validation

The following figures show the correlation between manual and automated orientation angles (Figure 2.18) in addition to the correlation between inter-rater orientation angles (Figure 2.19). It is important to note the range of each axis when interpreting these plots. In order to correct for angle sign discrepancies, a correction was applied to the data so that the smallest difference between two angles was considered. Correlations with orientation angles revealed significant positive correlations between automated and manual annotations ($r = 0.89$, $p<0.0001$) as well as inter-rater correlations ($r = 0.91$, $p<0.0001$). Figure 2.20 demonstrates the relationship between the eccentricity of an individual neuron compared to its manually annotated orientation angle. Due to the nature of the varying shape of neurons, eccentricity of a neuron combined with its angle of orientation, can be more predictive of directionality compared to orientation angle alone. Figure 2.21 depicts a vector image of the eccentricity-weighted orientation to further illustrate this relationship within the cortex.

www.manaraa.com

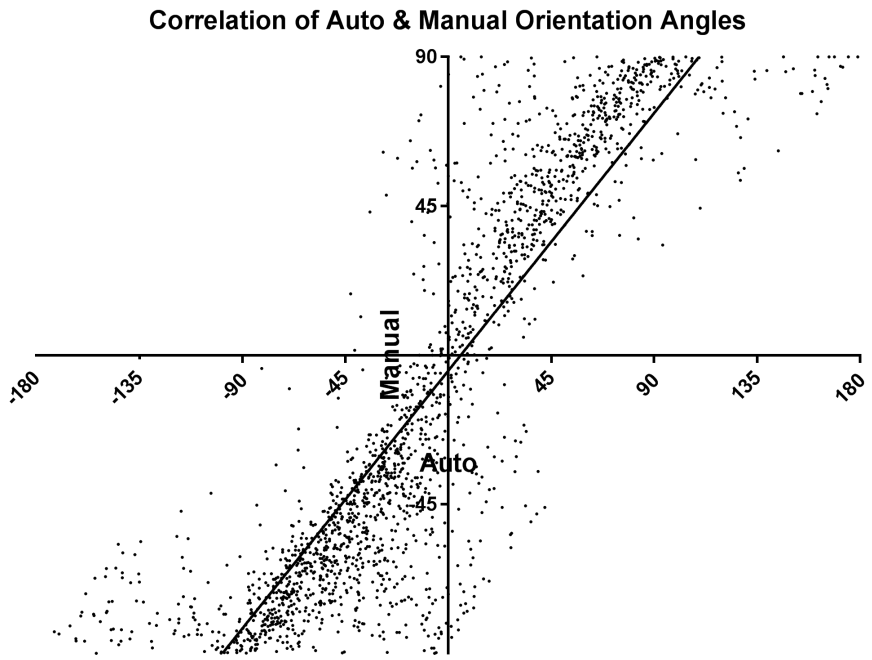

Figure 2.18: Spearman correlation of automated and manually annotated orientation angles; r = 0.89 p<0.0001

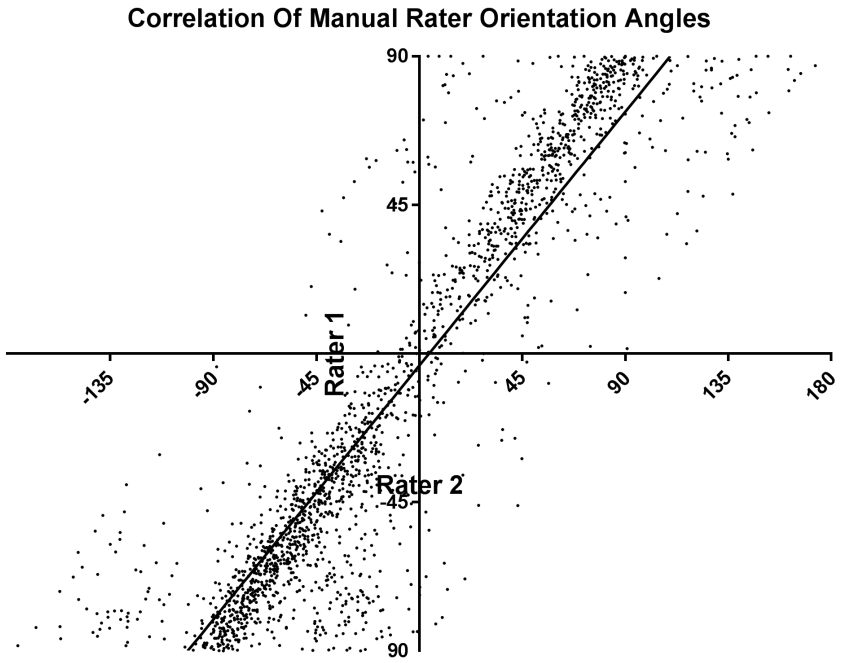

Figure 2.19: Spearman correlation of manually annotated orientation angles of two raters; r = 0.91 p<0.0001

www.manaraa.com

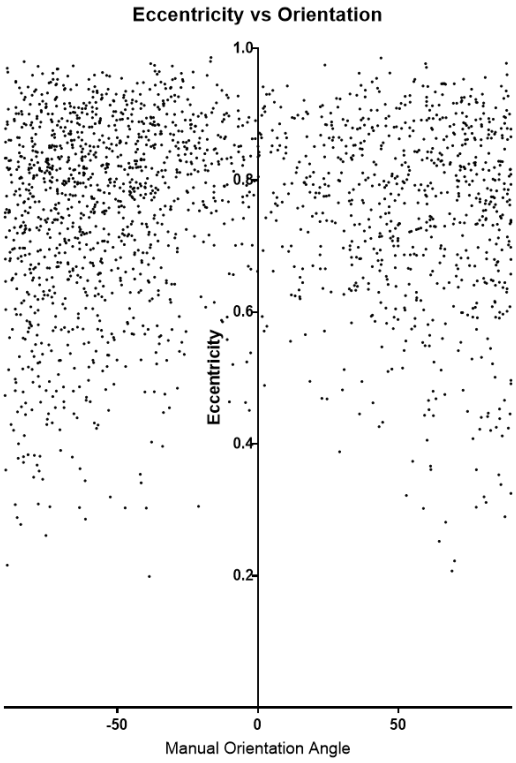

Figure 2.20: Orientation angle plotted against Eccentricity

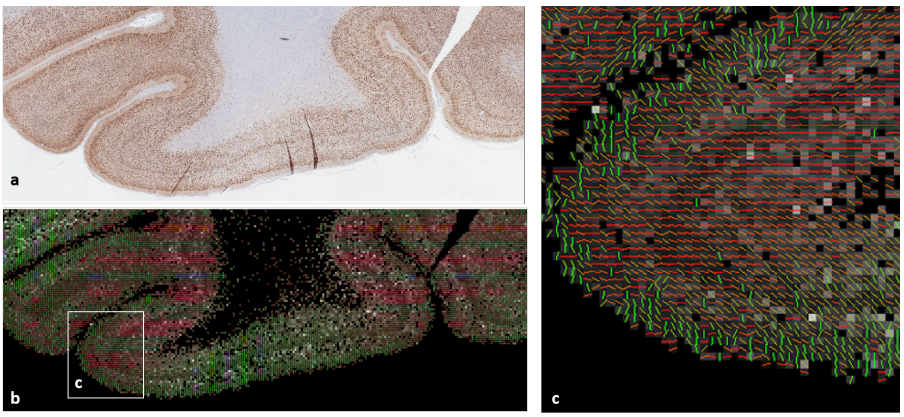

Figure 2.21: a) NEUN stained image - EPI_P036 b)Vector image of the eccentricity-weighted orientation plotted against neuron size feature map. c) Magnified view from image b. The green lines are average orientation angles in vertical direction, red lines are horizontally oriented angles

www.manaraa.com

2.3.4 Clinical Applications

The ANOVA analysis suggests that size, eccentricity and field fraction are all predictive of cases of focal cortical dysplasia within regions of tissue. However, all features are useful in the prediction of layering with the cortical architecture and may be used to further our current understanding of laminar patterns in the neocortex. The ANOVA analysis indicates that eccentricity is the most useful feature indicative of dysplasia and suggests that neuron morphology is the biggest factor in assessing abnormalities within cortical tissue. Orientation was the least indicative of FCD and may be due to the whole-slide analysis rather than specific regions, such as temporal pole areas, even with variance taken into consideration. Therefore, a more locally focused analysis may be necessary to better utilize the orientation metric.

Source	Feature	Corrected P	Layer
FCD	Density	0.02772	
	Size	0.0496*	L6
	Orientation Variance	0.2772	
	Clustering	0.2637	
	Eccentricity	0.0144*	L1
	Field Fraction	0.0280*	L6
Layer	Density	<0.0001*	
	Size	<0.0001*	
	Orientation Variance	0.1180	
	Clustering	<0.0001*	
	Eccentricity	<0.0001*	
	Field Fraction	<0.0001*	

Table 2.5: Two-way ANOVA results with a p-value corrected with Holm Bonferroni method. * denotes significance. For those features with significance in determining FCD, the last column indicates the most informative layer

www.manaraa.com

2.4 Discussion

2.4.1 Segmentation & Feature Maps

Compared to manual segmentation, automated cell segmentation and analysis offers several advantages, including the unbiased selection of cells, and the ability to extract large amounts of quantitative data cell image data sets with large number of images. However, both manual and fully automated analysis routines can lead to potential problems in assessing measurement uncertainty quantifying the stain intensity within cells. These problems include both over- and under-segmentation and overlap of cells due to the the 2-D histology sections. Therefore, the automated segmentation algorithm performed on the histology images were validated by comparing results with data from slides that were also manually segmented.

The performed experiments show that the proposed segmentation algorithm produces good results for most of the histology images used within this study. However, it is important to consider that segmentation results also depend on the quality of preparation and on the staining of histology images. Major challenges to this segmentation are the irregularity of staining however the automated segmentation localizes these areas by colour deconvolution in order to isolate the DAB stain. The results show that the obtained binary images from the watershed algorithm can be used for measurements of cell characteristics. In terms of the segmentation performance, the image characteristics that led to most neuron detection errors were high cell density, clustering and poor image contrast with noisy background.

In assessing the quality of the images produced in the feature maps, both neuron size and neuron density provide clear images of the cortical architecture, particularly when compared to the field fraction staining alone. The feature maps demonstrating neuron orientation, clustering and eccentricity prove to have less contrast with the laminar structure, however, these features are predicted to have a more localized benefit in assessing

www.manaraa.com

neuron integrity within the cortex.

2.4.2 Contouring Validation

The validation study performed to verify the accuracy and reproducibility generated satisfactory results in locating neurons within a histology slide. The DSC value is a simple and useful summary measure of spatial overlap, which can be applied to studies of reproducibility and accuracy in image segmentation. In comparing manual segmentations between two raters, the DSC value was greater than 0.7 in all cases, indicating a good overlap. We observed satisfactory results when comparing the spatial overlap between manual and automated segmentations, with only one instance of a slide having a DSC $>$ 0.7 [20]. This indicates firstly that the automated segmentation performs well compared with the manual annotations but also that the protocol used for manual annotations is reproducible and provides a accurate way to delineate neurons within a slide.

Additionally, several Bland-Altman plots were generated in order to analyze any bias between the two methods (manual vs automated or inter-rater)and to estimate an agreement interval, within which 95% of the differences of the second method, compared to the first one. Both neuron size and neuron density metrics were used in this validation analysis.

The automated method of density compared to the manual segmentation performed very well as demonstrated in Section 2.3.2. This indicates that the automated segmentation is reliable as a measure of density within the cortex. The automation of calculating neuron size requires further improvements and the large bias in the current algorithm indicates over-segmentation and thus reduced cell size. In addition, since averages are taken and cells are not compared one-to-one, a lot of data demonstrating the size variability within various layers is lost. The basis of the usual histopathological stains are somewhat difficult to control in terms of intensity of colour (stain), from cell to cell and more so from section to section, although this may change with the advent of new gener-

www.manaraa.com

ations of automated stainers. Improvements and optimization of the initial thresholding operations within the segmentation algorithm would help to correct the disparity in size between the manual and automated methods.

Although the Bland-Altman plot suggests that the technique used in both cases of manual annotations is essentially equivalent, one potential source of error leading to inter-rater differences is the learning curve in segmentation and histology experience as Rater 2 received less training.

2.4.3 Orientation Validation

The results demonstrate a high correlation between orientation in both automated and manual annotations (0.89) and the inter-rater manual annotations (0.91). The applied correction to the angles skewed the data since the range on one set of angles is offset, however, the results are still interpretable and reliable, indicating that the two sets of orientation angles are highly correlated.

In addition, the eccentricity can also be used in coordination with orientation. The more eccentric a neuron is, the more likely the orientation measure will be reliable. Since these case are most likely pyramidal neurons, moving forward a more specific feature analysis would only include these neuron types to provide a more accurate representation of the directionality of neurons within a section of cortex. Using a eccentricity weighted orientation provides a more informative approach.

2.4.4 Clinical Applications

The ANOVA analysis suggests that size, eccentricity and field fraction are all predictive of cases of focal cortical dysplasia within regions of tissue. Since field fraction is used so often in literature this study validates its use as a predictor of abnormal cortex. Eccentricity also proved to be useful in the prediction of dysplasia and likely relates to abnormal neuron morphology within FCD cases. Further investigative studies of this measure and

www.manaraa.com

its ability to locate lesions should be highlighted in future work. In contrast, orientation variance was the least indicative of FCD and also was not able to distinguish layering with the cortex. This may be due to the whole-slide analysis rather than specific regions, therefore, a more locally focused analysis of orientation may be necessary to better utilize the orientation metric.

All features assessed, with the exception of orientation variance, can be considered as predictors of layering within the cortical architecture and may be used to further our current understanding of laminar patterns in the neocortex.

Layer 6 was the most predictive of FCD, within the features found to be significant, and supports the current literature findings that white matter/layer 6 boundaries may be poorly defined in FCD [27]. Additionally, Layer 1 was indicative of abnormal eccentricity in FCD cases. Although layer 1 typically contains only small granular cells that are round (eccentricity close to zero), the eccentricity value was higher in layer 1 of FCD cases compared to non-FCD patients, indicating potential abnormal neuron proliferation.

www.manaraa.com

Bibliography

[1] J. D. Webster and R. W. Dunstan, "Whole-Slide Imaging and Automated Image Analysis Considerations and Opportunities in the Practice of Pathology," *Veterinary Pathology Online*, p. 0300985813503570, Oct. 2013.

[2] S. H. Eriksson, S. L. Free, M. Thom, L. Martinian, M. R. Symms, T. M. Salmenpera, A. W. McEvoy, W. Harkness, J. S. Duncan, and S. M. Sisodiya, "Correlation of quantitative MRI and neuropathology in epilepsy surgical resection specimens and T2 correlates with neuronal tissue in gray matter," *NeuroImage*, vol. 37, no. 1, pp. 48–55, 2007.

[3] A. Muhlebner, R. Coras, K. Kobow, M. Feucht, T. Czech, H. Stefan, D. Weigel, M. Buchfelder, H. Holthausen, and T. Pieper, "Neuropathologic measurements in focal cortical dysplasias: validation of the ILAE 2011 classification system and diagnostic implications for MRI," *Acta Neuropathologica*, vol. 123, no. 2, pp. 259–272, 2012.

[4] S. H. Eriksson, S. L. Free, M. Thom, L. Martinian, and S. M. Sisodiya, "Methodological aspects of 3d and automated 2d analyses of white matter neuronal density in temporal lobe epilepsy," *Neuropathology and applied neurobiology*, vol. 32, no. 3, pp. 260–270, 2006.

[5] L. S. Hsieh, J. H. Wen, K. Claycomb, Y. Huang, F. A. Harrsch, J. R. Naegele, F. Hyder, G. F. Buchanan, and A. Bordey, "Convulsive seizures from experimental focal cortical dysplasia occur independently of cell misplacement," *Nature Communications*, vol. 7, p. 11753, June 2016.

[6] B. E. Porter, A. R. Judkins, R. R. Clancy, A. Duhaime, D. J. Dlugos, and J. A. Golden, "Dysplasia A common finding in intractable pediatric temporal lobe epilepsy," *Neurology*, vol. 61, pp. 365–368, Aug. 2003.

www.manaraa.com

[7] G. A. Orban, *Neuronal Operations in the Visual Cortex*. Springer Science & Business Media, Dec. 2012.

[8] A. McKay Hart, T. Brannstrom, M. Wiberg, and G. Terenghi, "Primary sensory neurons and satellite cells after peripheral axotomy in the adult rat: timecourse of cell death and elimination," *Experimental Brain Research*, vol. 142, pp. 308–318, Feb. 2002.

[9] Y. Al-Kofahi, W. Lassoued, W. Lee, and B. Roysam, "Improved Automatic Detection and Segmentation of Cell Nuclei in Histopathology Images," *IEEE Transactions on Biomedical Engineering*, vol. 57, pp. 841–852, Apr. 2010.

[10] A. C. Ruifrok and D. A. Johnston, "Quantification of histochemical staining by color deconvolution," *Anal Quant Cytol Histol*, vol. 23, no. 4, pp. 291–299, 2001.

[11] A. C. Ruifrok, R. L. Katz, and D. A. Johnston, "Comparison of Quantification of Histochemical Staining By Hue-Saturation-Intensity (HSI) Transformation and Color-Deconvolution," *Applied Immunohistochemistry & Molecular Morphology*, vol. 11, no. 1, 2003.

[12] F. Meyer and S. Beucher, "Morphological segmentation," *Journal of Visual Communication and Image Representation*, vol. 1, pp. 21–46, Sept. 1990.

[13] F. Ajala, O. Fenwa, and M. Aku, "A comparative analysis of watershed and edge based segmentation of red blood cells," *International Journal of Medicine and Biomedical Research*, vol. 4, no. 1, pp. 1–7, 2015.

[14] H. P. Ng, S. H. Ong, K. W. C. Foong, P. S. Goh, and W. L. Nowinski, "Medical Image Segmentation Using K-Means Clustering and Improved Watershed Algorithm," in *2006 IEEE Southwest Symposium on Image Analysis and Interpretation*, pp. 61–65, 2006.

www.manaraa.com

[15] V. Grau, A. U. J. Mewes, M. Alcaniz, R. Kikinis, and S. K. Warfield, "Improved watershed transform for medical image segmentation using prior information," *IEEE Transactions on Medical Imaging*, vol. 23, pp. 447–458, Apr. 2004.

[16] M. Hildebrandt, T. Pieper, P. Winkler, D. Kolodziejczyk, H. Holthausen, and I. Blmcke, "Neuropathological spectrum of cortical dysplasia in children with severe focal epilepsies," *Acta Neuropathologica*, vol. 110, pp. 1–11, July 2005.

[17] L. R. Dice, "Measures of the Amount of Ecologic Association Between Species," *Ecology*, vol. 26, no. 3, pp. 297–302, 1945.

[18] R. E. Diaz and T. Sebastian, "Electromagnetic limits to radiofrequency (RF) neuronal telemetry," *Scientific Reports*, vol. 3, p. 3535, Dec. 2013.

[19] P. A. Yushkevich, J. Piven, H. C. Hazlett, R. G. Smith, S. Ho, J. C. Gee, and G. Gerig, "User-guided 3d active contour segmentation of anatomical structures: Significantly improved efficiency and reliability," *NeuroImage*, vol. 31, pp. 1116–1128, July 2006.

[20] A. P. Zijdenbos, B. M. Dawant, R. A. Margolin, and A. C. Palmer, "Morphometric analysis of white matter lesions in MR images: method and validation," *IEEE Transactions on Medical Imaging*, vol. 13, pp. 716–724, Dec. 1994.

[21] J. M. Bland and D. G. Altman, "Comparing methods of measurement: why plotting difference against standard method is misleading," *The Lancet*, vol. 346, pp. 1085–1087, Oct. 1995.

[22] M. M. Mukaka, "A guide to appropriate use of Correlation coefficient in medical research," *Malawi Medical Journal*, vol. 24, pp. 69–71, Jan. 2012.

[23] C. Spearman, "Footrule for Measuring Correlation," *British Journal of Psychology, 1904-1920*, vol. 2, pp. 89–108, July 1906.

www.manaraa.com

[24] S. Holm, "A Simple Sequentially Rejective Multiple Test Procedure," *Scandinavian Journal of Statistics*, vol. 6, no. 2, pp. 65–70, 1979.

[25] J. Chalfoun, M. Kociolek, A. Dima, M. Halter, A. Cardone, A. Peskin, P. Bajcsy, and M. Brady, "Segmenting time-lapse phase contrast images of adjacent NIH 3t3 cells," *Journal of Microscopy*, vol. 249, pp. 41–52, Jan. 2013.

[26] T. Chankong, N. Theera-Umpon, and S. Auephanwiriyakul, "Automatic cervical cell segmentation and classification in Pap smears," *Computer Methods and Programs in Biomedicine*, vol. 113, pp. 539–556, Feb. 2014.

[27] K. Blackmon, R. Kuzniecky, W. B. Barr, M. Snuderl, W. Doyle, O. Devinsky, and T. Thesen, "Cortical Gray-White Matter Blurring and Cognitive Morbidity in Focal Cortical Dysplasia," *Cerebral Cortex (New York, N.Y.: 1991)*, vol. 25, pp. 2854–2862, Sept. 2015.

www.manaraa.com

Chapter 3

Conclusions

The focus of this thesis is to investigate quantitative histological features within the temporal lobe neocortex of patients suffering from drug-resistant epilepsy. This relied on the development and validation of a segmentation pipeline to individually delineate neurons in histopathology specimens and extract relevant features from the segmented slides. Most importantly, I also demonstrated that quantitative histology features can predict focal cortical dysplasia (FCD) pathology in addition to the cortical laminar structure.

Automatically predicting focal cortical dysplasias from histological tissue specimens has the potential to reduce pathology workflow and the research undertaken in this thesis lays the groundwork for the non-invasive localization of pathology.

3.1 Limitations & Future Work

The global hypothesis of this thesis is that the signatures provided by quantitative histology features are able to predict abnormal pathology and with the correlation of MRI, histology and other diagnostic tools, the goal is to ultimately provide guidance to the neurosurgeon both prior to and during surgery. There are numerous future directions necessary to assist surgeons in localizing and resecting the seizure focus and the key to identifying epileptogenic abnormalities relies heavily on a multi-parametric approach.

www.manaraa.com

Using quantitative analysis techniques, the various pathologies and abnormalities of the histopathology in epilepsy lesions can be characterized into digital histology signatures and correlated with MRI. Further MRI-histology in-vivo correlation studies are necessary in pre-operative visualization and planning. Furthermore, correlation with functional data such as scalp or intracranial EEG could be used to validate and better understand the relationship between MR imaging, histological features and seizure propagation in the brain.

SVM training is required to further automate and predict FCD in epilepsy and increased patient dataset would be required to effectively create a pathology prediction machine. It would also be beneficial to include control tissue from non-epilepsy cases in order to refine the process and increase the accuracy of prediction. This presents a challenge, since acquiring histological brain tissue from healthy subjects is not possible. Older tissue samples are available, however, even with preservation efforts, tissue does not perform the same as fresh samples recived directly from surgical resections. For this reason accurate correlation between healthy and abnormal tissue is difficult.

In addition to an increased patient set, the inclusion of more neuron and FCD related features would allow for a better analysis at both a neuronal and laminar level. For example, this research focused features primarily related to Type I FCD, while the analysis of features relating to FCD type II and II, such as radial microcolumns and WM neurons, is necessary. It is also of great importance to correlate the presented histology findings with seizure outcome and MRI-negative TLE patients need to be examined with multiparametric MRI and quantitative histology validate the effectiveness of these techniques in lesion detection for this subset of patients. Data would be fed into a machine learning algorithm that determines histological features that correspond to feautures within MRI. This algorithm will learn the optimal set of feature in a cross-validated manner to create predictive histology that can help guide the location of epileptogenic lesions pre-operatively, thus improving resection and surgical outcomes.

www.manaraa.com

Appendix A

Neuron Contouring Protocol

A.1 Contour Specifications

- Manual contours should be performed in ITK-Snap software
- Use only one layer for labelling and set the Paintbrush tool to Shape round and size 2
- Do not include any neurons that touch the edge of the ROI
- Only those cells that appear as neurons and are stained dark brown should be included in the segmentation, as defined below:

1. Size:

    - The size of the neuron should be at a minimum, 4um in diameter and at a maximum, 70um in diameter, although these larger neurons are rare. If you are unsure of this measurement, the diameter of a neuron can be checked in the Aperio ImageScope software with the ruler tool. See Figure 1 for reference. The image resolution settings should be set to 0.5 microns/pixel and 20X magnification.

2. Morphology:

www.manaraa.com

- The neurons will be either pyramidal or granular neurons. Pyramidal cells are neurons with a large pyramidal shaped cell body and two dendritic trees which emerge from both the base and apex of the cell. Granular cells are small polymorphic neurons. Most of these neurons will be round or oval although may also have a star-shaped appearance due to dendritic projections.
- Features of a possible neuron may include the presence of dendrites or other projections and a cell nucleus
- Attached neurons that fit all other criteria should be counted and contoured as multiple, separate neurons. Neurons may appear overlapped with other cells, neural debris, or artifacts. In these cases, contour the neuron as best possible, ignoring the other objects within the slide.
- Do not include neurons that are very irregular in shape and have none of the above mentioned features of a neuron.
- In addition, do not include the full dendritic branch in the contour. The dendrite may be included in cases where the NEUN stain in these regions is as intense as other areas of the cell body. This may mean including only a small part of the dendritic branch.

3. Staining

- Neurons should be evenly stained and the cell body mostly homogenous in colour. The cell nucleus, if visible, will be stained with more intensity than the rest of the neuron.
- Very light brown or blue stained cells should not be included in the contour.

www.manaraa.com

Appendix B

Neuron Orientation Protocol

B.1 Region of Interest

- The regions of interest (ROI) defined from previous annotations will be used
- Load both ROI and one set of previous contour annotations into ITK-Snap software. The previous segmentation should be loaded as an overlay and the opacity adjusted as needed.

B.2 Annotation Specifications

- Manual orientation annotations should be performed only on previously annotated neurons. If a cell was not selected as a neuron previously, do not annotate with orientation.
- Use label 2 for the new annotations and set the Paintbrush tool to Shape round and size 3 with the isotropic option checked off.
- To perform the annotation, draw a straight line through the centre of the cell body
  - In pyramidal cells:

www.manaraa.com

    * The primary dendritic branch should be used to decide the orientation, running from base to apex.
    * If there is not a visible dendritic branch use the general morphology of the neuron to decide the orientation. This should be based on the longest axis.

  – In granular cells:

    * First consider the presence of any dendritic processes and use those to assist in annotating the orientation.
    * Next the morphology of the cell should be assessed and the orientation can be considered as the diameter in the longest direction.
    * If none of these factors indicate the orientation, the orientation of surrounding cells should be considered.

- Note: The orientation line may go outside the border of the cell provided that it does not enter the boundary of another neuron.
- Save the segmentation into the orientation folder

www.manaraa.com

Appendix C

Layer Segmentation Protocol

C.1 Label Specifications

- Manual contours should be performed in Aperio ImageScope Software
- The slide should only be labelled in areas that can be considered non-tangential cuts and within the plane of the slide, in addition, any areas with staining artifacts should be excluded.
- Layer 1 is outlined first and starts from above the pial as initial reference. This layer should extend down through the cortex to lower layers. This process is repeated for each layer, using layer markers such as the contrast of dense neurons to guide the user in manually annotating the layers.
- Each layer should overlap from the previous layer such that no space is created between the layers, while still maintaining the boundaries. This overlap is accounted for and removed in post-processing of the layers, before final analysis in MATLAB.
- Layer 6 is the final layer and should extend further than all other layers but still stay as much out of the white matter as possible.

www.manaraa.com

- The resulting .xml annotation files are converted to readable MATLAB data for further analysis.

www.manaraa.com

Curriculum Vita

Charlotte Blinston, B.Cmp.H.

Imaging Research Laboratories
Robarts Research Institute

EDUCATION

Sept. 2012 – present
Master of Engineering Science (*Candidate*)
Biomedical Engineering Graduate Program
Western University, London, Ontario, Canada
Supervisors: Terry Peters, Ph.D, Ali Khan, Ph.D
Thesis: "Histological Quantification in Temporal Lobe Epilepsy"

Sept. 2008 – June 2012
Bachelor of Computing, Honours
Specialization in Biomedical Computer Science
Queen's University, Kingston, Ontario, Canada
Undergraduate Project: "Analysis of sensorimotor dysfunction in stroke subjects"

POSITIONS

Jan. 2013 – April 2014
Lead Graduate Teaching Assistant
ES1036B: Programming Fundamentals for Engineers (C++)
Department of Electrical and Computer Engineering
Western University, London, Ontario, Canada

June 2012 – Sept. 2012
Summer Student
Department of Knowledge and Innovation
Chatham Kent Health Alliance, Chatham, Ontario, Canada

Sept. 2011 – May 2012
Undergraduate Research Assistant
Molecular Scene Analysis Laboratory
School of Computing, Queen's University, Kingston, Ontario, Canada
Supervisor: Janice Glasgow, Ph.D.
Project: "Analysis of sensorimotor dysfunction in stroke subjects"

May 2011 – Sept. 2011
Undergraduate Summer Research Assistant
Molecular Scene Analysis Laboratory
School of Computing, Queen's University, Kingston, Ontario, Canada
Supervisor: Janice Glasgow, Ph.D.
Project: "Design, implementation and evaluation of a case-based reasoning system for the diagnosis of impairment and for the planning of rehabilitation strategies for patients with stroke".

www.manaraa.com

ACADEMIC AWARDS and SCHOLARSHIPS

Sept. 2012 – Aug. 2014 **Western Graduate Research Scholarship**
Awarded to a full time graduate student for tuition support who has maintained an average of 80% or more

May 2011 **Ian Lawson Van Toch Summer Research Fellowship in Biomedical Computing**
Awarded to a student in the Biomedical Computing program at Queen's University in order to complete summer research

Sept. 2008 – June 2012 **Queen's University Excellence Scholarship**
Awarded upon admission to Queen's students who have an admission average of 90.0 - 94.9%

Sept. 2008 **The Queen Elizabeth II Aiming for the Top Scholarship**
Awarded to students who have shown academic excellence at the high school level

PUBLISHED JOURNAL MANUSCRIPTS (1)

1. Goubran, M., Bernhardt, B. C., Cantor-Rivera, D., Lau, J. C., **Blinston, C**., Hammond, R. R., de Ribaupierre, S., Burneo, J. G., Mirsattari, S. M., Steven, D. A., Parrent, A. G., Bernasconi, A., Bernasconi, N., Peters, T. M., Khan, A. R., "*In vivo MRI signatures of hippocampal subfield pathology in intractable epilepsy*". Human Brain Mapping 2016; 37 (3): 1103-1119

ORAL PRESENTATIONS (1) ***presenter***

1. **C. Blinston***, M. Goubran, T. Peters, R. Hammond, A.R. Khan. "*Imaging Techniques for Histology Quantification in Medically Intractable TLE*". LHSC Epilepsy Research Day, London, Ontario, Canada (Nov 4 2016)

2. **C. Blinston**, M. Goubran*, T. Peters, R. Hammond, A.R. Khan. "*Computational imaging techniques for neuron-specific quantification of cortical architecture in temporal lobe epilepsy*". London Imaging Discovery Day, London, Ontario, Canada (June 26 2014)

POSTER PRESENTATIONS (5)

1. **C. Blinston**, T. Peters, R. Hammond, A.R. Khan. "*Computational Imaging Techniques for Histological Quantification of Cortical Architecture in Epilepsy*". Imaging Network Ontario Symposium, Toronto, Ontario, Canada (March 24-25 2014)

www.manaraa.com

2. **C. Blinston**, T. Peters, R. Hammond, A.R. Khan. "*Computational Imaging Techniques for Histological Quantification of Cortical Architecture in Epilepsy*". London Health Research Day, Schulich School of Medicine and Dentistry, Western University, London, Ontario, Canada (March 18 2014)

3. **C. Blinston**, R. Hammond, M. Goubran, A. Parrent, J.G. Burneo,S. De Ribaupierre, D. Steven, T. Peters, A. R. Khan. "*Quantitative analysis of neocortical architecture in refractory temporal lobe epilepsy*". American Epilepsy Society Annual Meeting, Washington, D.C., USA (Dec 8 2013)

4. **C. Blinston**, T. Peters, R. Hammond, A.R. Khan. "*Quantitative characterization of neuropathology in temporal lobe epilepsy*". London Health Research Day, Schulich School of Medicine and Dentistry, Western University, London, Ontario, Canada (March 19 2013)

5. **C. Blinston,** K. Tyryshkin, J. Glasgow. "*Analysis of sensorimotor dysfunction in stroke subjects*". Creative Computing: Art, Games, Research. School of Computing, Queen's University, Kingston, Ontario, Canada (April 5 2012)

PROFESSIONAL MEMBERSHIPS

2013 - Present	Biomedical Engineering Society, **Student Member**
	IEEE Membership, **Student Member**
	IEEE Women in Engineering Membership, **Student Member**

RELEVANT GRADUATE COURSES

Biomedical Engineering Graduate Program, Western University, London, Ontario, Canada

Jan 2015 – April 2015	VASCPROG 9603	Research Ethics And Biostatistics
Jan. 2013 – April 2013	BME 9511	Image-Guided Interventions
	BME 9550	Principles of Communication and Knowledge Translation for Biomedical Engineers
Sep. 2012 – Dec. 2012	BME 9509	Digital Image Processing
	BME 9501	Introduction to Biomedical Engineering

www.manaraa.com